NASA-CR-152, 046

FINAL TECHNICAL REPORT

DEVELOPMENT OF DOPED-GERMANIUM PHOTOCONDUCTORS FOR ASTRONOMICAL OBSERVATIONS AT WAVELENGTHS FROM 30 TO 120 MICROMETERS

Contract No. NAS2-9385

For - National Aeronautics and Space Administration
Ames Research Center
Moffett Field, CA 94035

SANTA BARBARA RESEARCH CENTER
A Subsidiary of Hughes Aircraft Company
SBRC

NASA-CR-152, 046

SANTA BARBARA RESEARCH CENTER

A Subsidiary of Hughes Aircraft Company

75 COROMAR DRIVE, GOLETA, CALIFORNIA

FINAL TECHNICAL REPORT

DEVELOPMENT OF DOPED-GERMANIUM PHOTOCONDUCTORS FOR ASTRONOMICAL OBSERVATIONS AT WAVELENGTHS FROM 30 TO 120 MICROMETERS

Contract No. NAS2-9385

For

National Aeronautics and Space Administration
Ames Research Center
Moffett Field, CA 94035

31 October 1977

Prepared by P.R. Bratt
P. R. Bratt
Senior Scientist

and N.N. Lewis
N. N. Lewis
Project Engineer

Approved by L.E. Long
L. E. Long
Project Manager

PREFACE

This report describes the results of a technology development program directed toward the optimization of the performance of beryllium-doped germanium (Ge:Be) and gallium-doped germanium (Ge:Ga) infrared detectors operating near 3°K at low backgrounds (10^8 photons/sec/cm^2) and low frequencies (≥ 0.05 Hz). The work was performed at the Santa Barbara Research Center over the period from 1 October 1976 to 31 March 1977.

The Project Manager during the first half of the work was Peter R. Bratt. During the second half, Lawrence E. Long undertook the management responsibility. The Project Engineer was Nancy N. Lewis. The Project Technical Monitor for NASA/Ames was Craig McCreight. A number of other people at SBRC made significant contributions to this project. Roger A. Cole and Eugene D. Van Orsdell grew the Ge:Ga and Ge:Be crystals. Kurt R. Winrich, David J. Calhoun, and James B. Knutsen made the Hall effect measurements and data analysis. Beulah L. Marolf fabricated detectors, and Courtney W. Manker and Fred J. Strobach assisted in the design and assembly of the low-background test fixtures. Richard L. Nielsen provided valuable assistance in trouble shooting test problems and evaluation of test results. We are also indebted to W. J. Moore of the U. S. Naval Research Laboratories for helpful suggestions during the course of this work.

CONTENTS

CONTENTS (Cont)

ILLUSTRATIONS

ILLUSTRATIONS (Cont)

ILLUSTRATIONS (Cont)

TABLES

Section 1
INTRODUCTION AND SUMMARY

The work described in this report was a continuation of a previous technology development program on Ge:Be and Ge:Ga detectors which was funded by NASA/Goddard and administered by Kitt Peak National Observatory. During the previous phase of this work, emphasis was on Ge:Ga detector development. During this new phase, more emphasis was placed on Ge:Be detector development.

The ultimate goal of this work was to develop the technology for production of doped-germanium detectors which have optimized performance in the 30- to 120-μm wavelength range and are capable of achieving the objectives of the Infrared Astronomy Satellite (IRAS) space mission.

Because of the short period of performance for the work performed on this phase, it was not expected that the technology for producing fully optimized detectors would be totally developed. However, significant advancement was anticipated. A future development phase is considered to be necessary to continue the development work.

The work of this phase was divided into the following major tasks:

1. Growth of Ge:Ga crystals from high-purity starting material with Ga concentrations different from that previously produced, and development of a zone leveling method to produce a uniform Ga doping concentration.
2. Growth of uncompensated Ge:Be crystals from high-purity starting material with a range of Be concentrations between 1×10^{14} and 1×10^{16} atoms/cm^3.
3. Evaluation of crystals by means of Hall effect and resistance measurements as a function of temperature.
4. Fabrication and test of detectors made from both Ge:Be and Ge:Ga crystals to determine the relative performance between different crystals. Correlation of detector test data with material evaluation data and analysis of how to further optimize detector performance.

All these tasks were successfully completed during the course of the program. The results of this phase may be summarized as follows:

The zone leveling technique for growing Ge:Ga crystals was implemented and shown to produce a uniform Ga doping concentration over more than 5 inches of ingot length. This established a reliable material production method which yields a quantity of detector material more than adequate for the IRAS focal plane array (FPA) fabrication.

Ge:Ga detectors made from the zone leveled material showed somewhat lower NEP values than any made previously at SBRC. The best measured NEP was 4×10^{-17} watts/Hz$^{\frac{1}{2}}$ at a wavelength of 100 μm, a frequency of 1 Hz, an operating temperature of 3.0°K and a background flux of 4×10^{8} photons/sec/cm^2.

Tests on a number of Ge:Ga detectors showed a high yield of good elements and excellent uniformity between different elements. The detector fabrication technology appears to be adequate for fabrication of a large focal plane array such as that required for the IRAS mission.

Growth of Ge:Be crystals proved to be difficult because of small amounts of oxygen in the zone melting furnace which either formed a Be-O compound on the surface of the ingot or a Be-O complex inside the ingot. In either case, Be is effectively removed to an inactive site and cannot produce impurity photoconductivity. The problem was solved by growing Ge:Be crystals under vacuum. This yielded a small amount of material for detector test and evaluation; however, uniformly doped Ge:Be ingots were not obtained, and the control of Be doping concentration was not as good as for Ga doping. Further work on the Ge:Be crystal growth technology is warranted.

The maximum limit on Be doping concentration established by impurity hopping conductivity was determined to be $2\text{-}3 \times 10^{15}$ atoms/cm^3.

Ge:Be detectors made on this program achieved NEP values of 3×10^{-16} watts/Hz$^{\frac{1}{2}}$ at a wavelength of 40 μm, a frequency of 1 Hz, an operating temperature of 3.0°K, and a background flux of 7×10^{8} photons/sec/cm^2.

The yield of Ge:Be detectors was acceptable. However, these detectors do not seem to be operating as close to the theoretical background limited performance (BLIP) standard as do the Ge:Ga detectors.

In general, it may be concluded from this work that Ge:Ga development is essentially complete, and this material should adequately serve for the long-wavelength detector array in the IRAS FPA. Minor technology improvements such as a slightly higher Ga doping concentration and the use of integrating cavities should further improve detector performance.

Work on Ge:Be is not complete. Further development of the crystal growth technology is necessary to have a reliable doping method. It is also of interest to grow compensated Ge:Be crystals and compare detector performance to the uncompensated material that has been used up to this point in time.

Section 2
REVIEW OF PREVIOUS WORK

Previous work involved exploratory development in Ge:Ga crystal growth as well as detector fabrication technology using both Ge:Ga and Ge:Be material. Ge:Ga detectors were made from material furnished by the Naval Research Laboratories (W. J. Moore) and from material produced at SBRC. Ge:Be detectors were made only from material furnished by NRL. The results of the Ge:Ga work were very encouraging in that the crystal growth method used was shown to be capable of producing a specified Ga doping concentration with very low concentrations of residual donor impurities. Detector performance was found to be reasonably good with NEP = 4×10^{-16} watt/$Hz^{\frac{1}{2}}$ at 100 μm for a background flux of 1.8×10^{10} photons/sec/cm^2, and 1.3×10^{-16} watt/$Hz^{\frac{1}{2}}$ for a background flux of 1.2×10^{9} photons/sec/cm^2. The Ge:Be detectors made from NRL material achieved an NEP of 1×10^{-15} watts/$Hz^{\frac{1}{2}}$ at 40 μm with a background flux of 1.9×10^{9} photons/sec/cm^2.

This work clearly demonstrated the feasibility of these detector materials as very sensitive detectors of long-wavelength radiation under low-temperature and low-background conditions of operation. It established a starting point from which further technology development efforts could proceed, and fostered a confidence that the ultimate performance goals could be realized within reasonable time and cost constraints.

The zone melting method for growth of Ge:Ga crystals was implemented and found to work well. After growth of a few crystals, it was realized that a more uniform Ga doping concentration should be attainable by going to a zone leveling modification using the same furnace. This became one of the primary tasks for the follow-on program. No previous experience with the growth of Ge:Be crystals existed at SBRC so this also became a major new task.

Detector fabrication technology which had been previously developed at SBRC for doped Ge detectors was found to work well on these longer wavelength materials. In particular, the use of ion implantation in the formation of electrical contacts to the crystals was shown to give an ohmic contact with little or no excess noise for frequencies down to 1 Hz.

The fundamental principles of operation of a doped-germanium far infrared detector were described in the Final Technical Report for the previous phase of this program.[1] The detector operates as an extrinsic photoconductor. Photoionization of the doping impurity atoms (Ga or Be) by infrared radiation produces extra free holes in the crystal which increase its conductivity. This conductivity increase can be easily measured using a suitable electrical circuit.

The energy required for ionization of the Ga atoms in Ge is 0.011 eV. Thus, incoming photons with an energy greater than this value can cause photoionization; those with a lesser energy cannot. This requirement can be expressed in terms of the infrared photon's wavelength as follows:

$$\frac{hc}{\lambda} \geq \epsilon_i \tag{1}$$

where h is Planck's constant, c the speed of light, λ is the wavelength, and ϵ_i is the ionization energy. For energies expressed in eV and wavelength in μm, Equation (1) can be rewritten as

$$\lambda \leq \frac{1.24}{\epsilon_i} \tag{2}$$

Thus, photons of wavelength less than 100 μm can produce photoconductivity in Ge:Ga crystals. The Be atom in Ge has an ionization energy of 0.024 eV. Therefore, photons of wavelength less than 52 μm can produce photoconductivity in Ge:Be crystals.

---

1. P. R. Bratt, "Improved Ge:Ga and Ge:Be Far Infrared Detector Development," Final Technical Report, Contract No. 86310 (AURA), Santa Barbara Research Center, Oct. 1977

The optimization of a detector's sensitivity involves an attempt to maximize the photoconductive response and minimize the various noise sources present either in the detector itself or in the associated electrical components.

A theoretical analysis of detector operation under low background conditions has pointed out the directions in which to proceed toward optimization of detector performance. These may be summarized as follows:

1. Grow Ge:Ga and Ge:Be crystals with doping concentrations as large as possible so as to maximize the responsive quantum efficiency, but keep the doping concentration below the point where impurity hopping conductivity begins to significantly lower detector resistance. This implies that there is some optimum doping concentration which will be different for each type of impurity atom. This concentration must be determined experimentally for the particular temperatures of operation and background photon flux levels expected in the IRAS mission.
2. Maximize the photoconductive gain of the detector by using material with long free-hole lifetime. This mandates the use of high-purity Ge starting material with a very low concentration of residual donor impurities. Fabricate detector crystals with a minimum interelectrode spacing and operate with applied electric field strength as large as possible.
3. Provide electrical contacts to the doped Ge crystal which do not produce excess noise and are "ohmic" for transport of charge carriers (free holes) into and out of the crystal.

These guidelines formed the basis for the development efforts to be carried out in the follow-on program described in this report.

Section 3
Ge:Ga CRYSTAL GROWTH AND EVALUATION

CRYSTAL GROWTH

One Ge:Ga crystal was grown during this phase of the program. A zone leveling technique was used in an attempt to provide a more uniform distribution of Ga in the crystal than was achieved in previous runs at SBRC. Also a higher doping concentration was used to see if material with a higher quantum efficiency could be obtained.

The method of Ge purification by multipass zone refining described in the previous report was used.[2] Ga doping by means of the pellet dropping spoon was also used. However, in this run, the doping pellet was dropped near the tail end of the ingot. The molten zone was formed there, moved to the seed end, then back to the tail end again, completing the run. Figure 3-1 shows a photograph of the finished Ge:Ga ingot. The seed end of the crystal (with seed still attached) is to the left in this picture, and the tail end is to the right. This crystal contains over 5 inches of uniformly doped material in the central region of the ingot. The seed end was subsequently cut off for reuse and the tail end was cut off and discarded as scrap.

DOPING CONCENTRATION

Samples were cut from the doped region at 1-inch intervals for evaluation by Hall effect measurements. The Ga doping concentration was found to be quite uniform over the whole 5-inch length which was evaluated. The results are shown in Figure 3-2. The average doping concentration was 2.5×10^{14} Ga atoms/cm^3. This provided high quality detector material with a doping concentration 2.5 times greater than that used in our previous work.

---

2. Op cit.

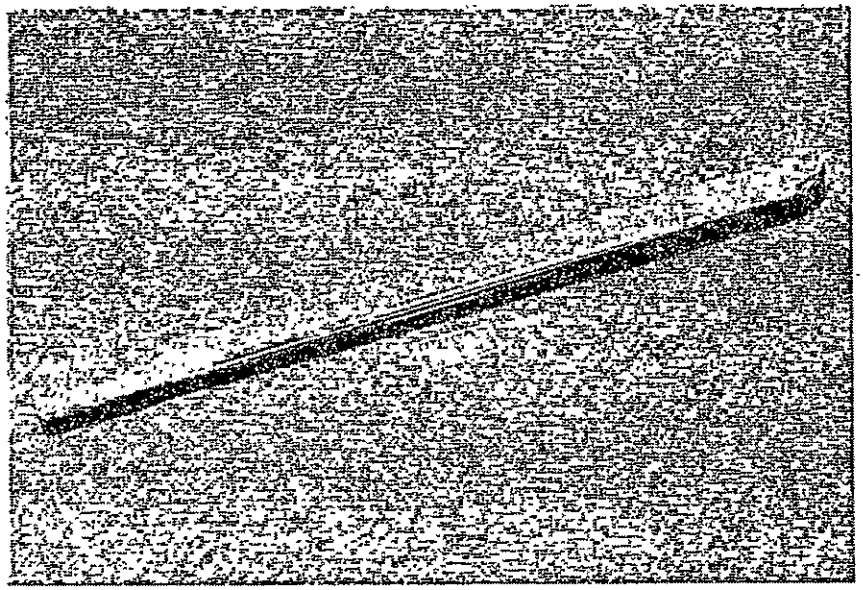

Figure 3-1. Ge:Ga Single Crystal Ingot No. 4

Note: The seed end is to the left and the tail end to the right. Over 13 cm of uniformly doped material is contained in the central region of this ingot.

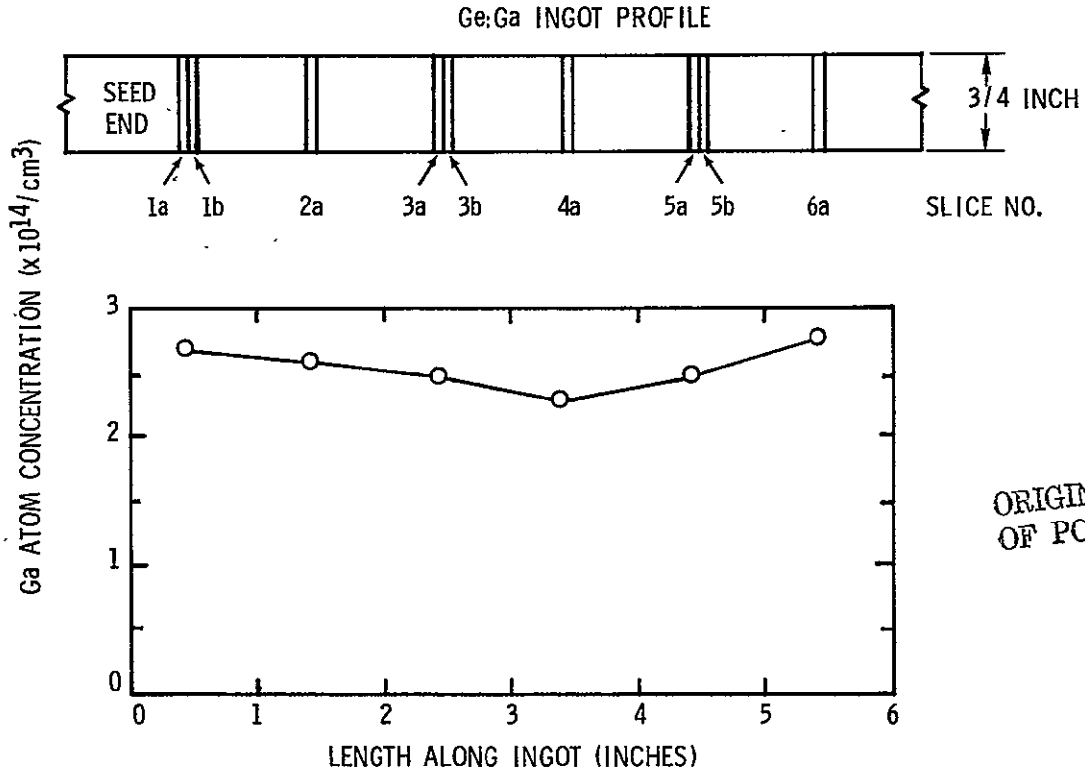

Figure 3-2. Doping Profile for Ge:Ga Ingot No. 4 Produced by a Zone Leveling Technique

Evaluation of selected samples by means of Hall effect measurements versus temperature was also done. Comparison of experimental data points with theoretically generated curves provides a determination of the residual donor atom concentration in the crystal. Details of the method of analysis were given in the previous report.[2] Figures 3-3 and 3-4 show experimentally measured Hall coefficient data versus temperature and the theoretical fit which was obtained for two of the three samples which were evaluated. The third sample, Ge:Ga No. 4-5a was almost identical in behavior to No. 4-3a and is, therefore, not shown. The last four low temperature experiemntal data points in Figure 3-3 are in error due to limitations in the Hall effect equipment and should be disregarded. The rise in the high-temperature data points above the theoretical line is due to the influence of a small population of high-mobility holes in the light mass valence band which cause the measured Hall coefficient to rise in this temperature range.[3] This could be eliminated by the use of higher magnetic field strengths in the Hall effect measurement, but our equipment was limited to a field strength of 5,000 gauss. The effect does not interfere with the low-temperature data, and thus does not compromise the theoretical curve fitting procedure.

Donor atom concentrations deduced from the comparison between theoretical and experimental data are listed in Table 3-1 for all three samples. It is to be noted that the residual donor atom concentration in this crystal is in the $10^{10}/cm^3$ range whereas previous Ge:Ga material had concentrations in the $10^{11}/cm^3$ range or higher. The free-hole lifetime in this material should, therefore, be higher than in any of the previously grown crystals.

The values of ionization energy are found to be somewhat higher than the literature value of 0.0108 eV. This result was also noted for our previous Ga-doped crystal, Ge:Ga 3. The reason for this is not presently known.

---

2. Ibid.

3. R. K. Willardson, T. C. Harman, and A. C. Beer, Phys. Rev. 96, 1512 (1954)

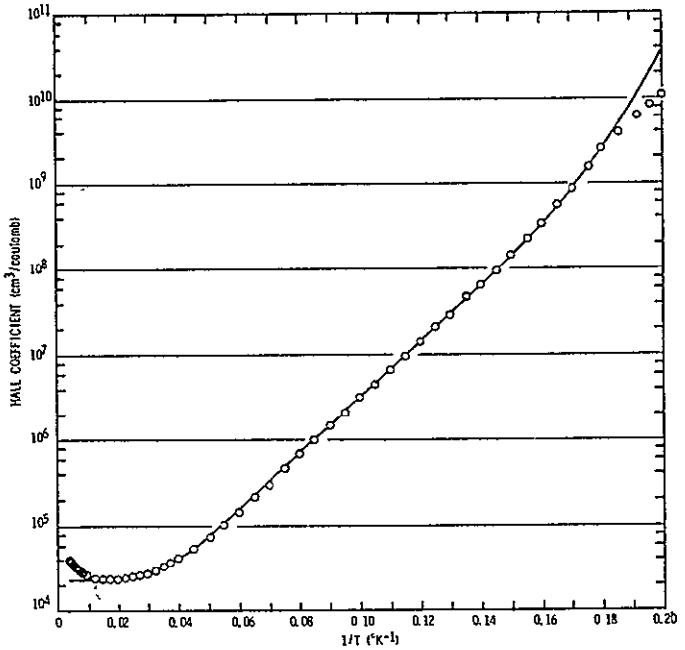

Figure 3-3. Hall Coefficient Versus Reciprocal Temperature for Sample No. Ge:Ga 4-1a

Note: Open circles are experimental data points, the solid line is theoretical data calculated using the parameters given in Table 3-1.

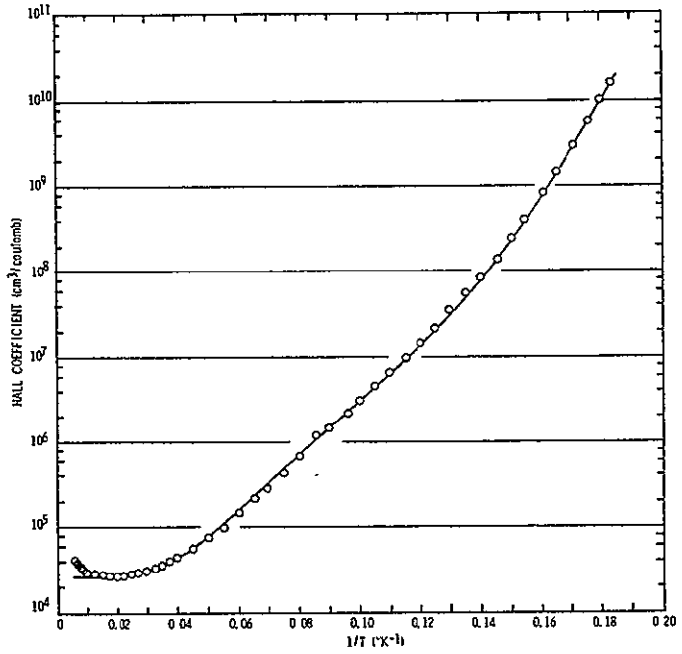

Figure 3-4. Hall Coefficient Versus Reciprocal Temperature for Sample No. Ge:Ga 4-3a

Note: Open circles are experimental data points, the solid line is theoretical data calculated using the parameters given in Table 3-1.

Table 3-1. Summary of Doping Parameters for Ge:Ga Crystal No. 4

Sample No.	$N_A - N_D$ (cm^{-3})	N_A (cm^{-3})	N_D (cm^{-3})	ϵ_i (eV)
	$\times 10^{14}$	$\times 10^{14}$	$\times 10^{10}$	
Ge:Ga 4-1a	2.7	2.7	1.4	0.0114
4-2a	2.6	-	-	-
4-3a	2.5	2.5	9.5	0.0112
4-4a	2.3	-	-	-
4-5a	2.5	2.5	8.0	0.0113
4-6a	2.8	-	-	-

HALL MOBILITY

The Hall mobility is plotted versus temperature in Figure 3-5 for all three of the samples cut from crystal Ge:Ga 4. It is seen that they all have essentially the same mobility values at all temperatures. There is some scatter in the data at temperatures below 7°K, particularly for sample 4-1a, which is thought to be due to experimental error. The data points for the other two samples continue rising down to the lowest temperature of 5.5°K.

No attempt was made to do a detailed analysis of the mobility data. Qualitatively, it appears that the hole mobility in these samples is primarily limited by lattice scattering because this is the only scattering mechanism which permits the mobility to continue to rise as temperature is lowered. Ionized impurity scattering produces a mobility which decreases as temperature is lowered and neutral impurity scattering causes the mobility to be nearly independent of temperature. At a low enough temperature, neutral impurity scattering would be expected to become predominant and limit further mobility increases.

An estimate of the neutral impurity limited mobility may be calculated from the formula of Sclar[4]

$$\mu_N = \frac{1.17 \times 10^{22}\,(m^*/m_o)}{K\,N_N}\left[0.734 \times 10^{-2}\,\frac{K\,T^{\frac{1}{2}}}{(m^*/m_o)^{\frac{1}{2}}} + \frac{30.2\,(m^*/m_o)^{\frac{1}{2}}}{K\,T^{\frac{1}{2}}}\right] \quad (3)$$

where m^* is the hole effective mass, m_o is the mass of an electron, K is the dielectric constant of Ge, N_N is the concentration of neutral scattering centers, and T is the absolute temperature.

Using

$m^*/m_o = 0.28$

$K = 16$

$N_N = 2.5 \times 10^{14}/cm^3$

we obtain values for μ_N in the vicinity of 8×10^5 cm^2/volt sec. These are plotted on Figure 3-5 for the temperature range between 2° and 10°K. It would not be unreasonable to assume that the measured data are approaching this limit. However, further measurements in the 2° to 6°K range would be required to establish this for certain.

RESISTANCE VERSUS TEMPERATURE

Because of equipment limitations, the variable temperature Hall effect measurements on Ge:Ga samples could not be extended below 5°K. This is not due to a temperature limitation, but because the sample impedance becomes so high that the constant current supply on the Hall apparatus no longer functions properly. To obtain data at temperatures less than 5°K, a Ge:Ga detector element was obtained and its resistance measured versus temperature over the range from 10° to 3°K. The main objective of this measurement was to determine if impurity hopping conductivity was present. Figure 3-6 shows the circuit diagram used for the measurement. Data were taken with a constant voltage of 0.02 volt applied across the sample producing

4. N. Sclar, Phys. Rev. 104, 1559 (1956)

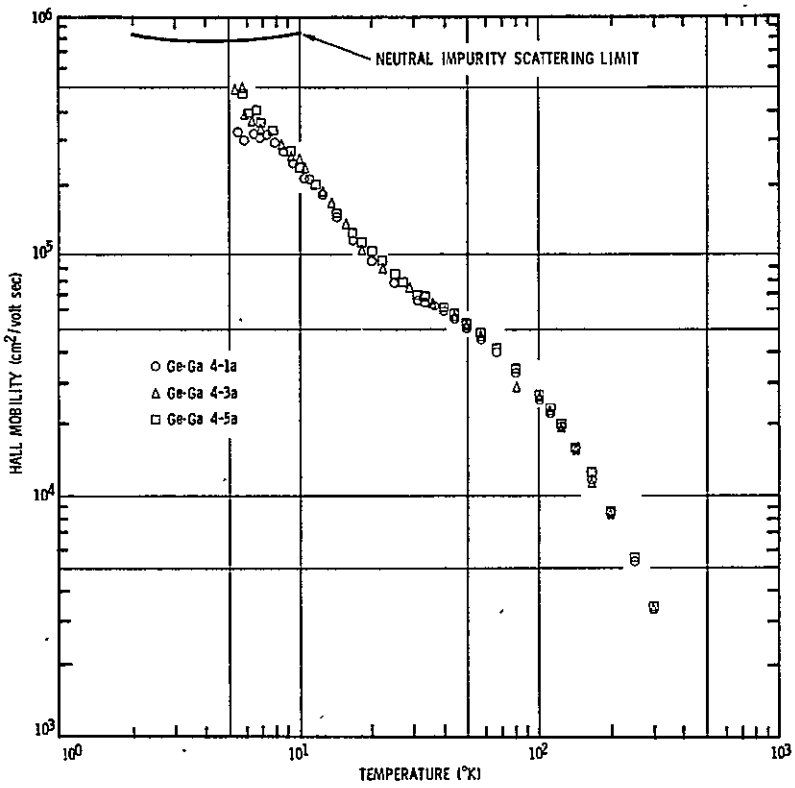

Figure 3-5. Hall Mobility Versus Temperature for Three Samples from Crystal Ge:Ga 4

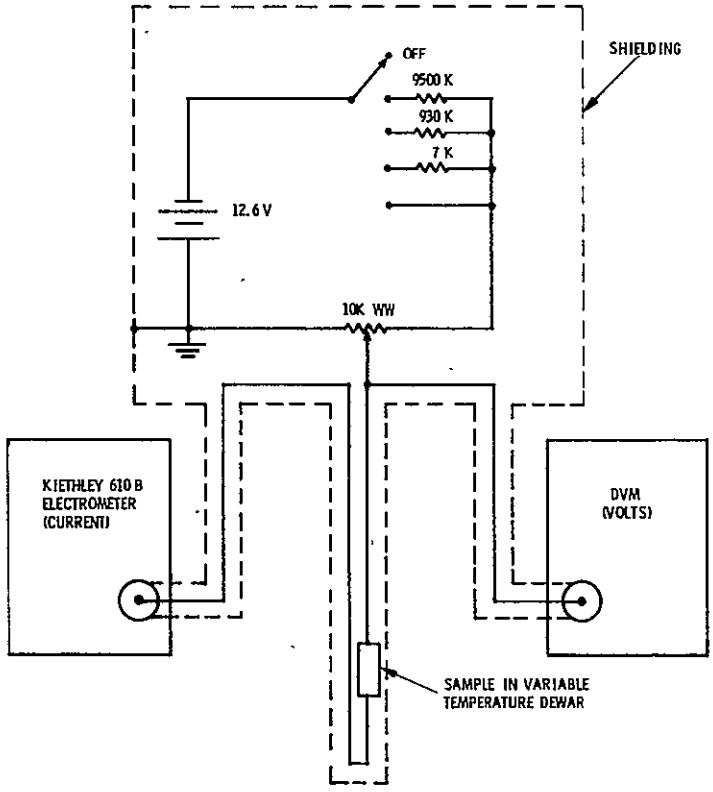

Figure 3-6. Circuit Used for Resistance Versus Temperature Measurements on Detector Samples

an electric field strength of 0.4 volt/cm. A carbon resistor thermometer mounted close to the detector sample was used for temperature measurement. Background radiation was excluded from the samples during the measurements.

Figure 3-7 shows the results on two samples from crystal Ge:Ga 4. These samples were taken from the same slice as were the detector samples. In fact, they were surplus detector samples and were, therefore, fabricated in the same manner as detector samples. One sample shows a strict exponential dependence for resistance versus 1/T up to 10^{12} ohms. The other sample shows a slight variation from an exponential dependence in the vicinity of 10^{11} ohms which may be due to some experimental error since, to obtain the highest resistance readings, currents in the 10^{-14} ampere range had to be measured. It is concluded from these data that impurity hopping conductivity is not a significant problem in these Ge:Ga samples with a Ga doping concentration of 2.5×10^{14} atoms/cm^3.

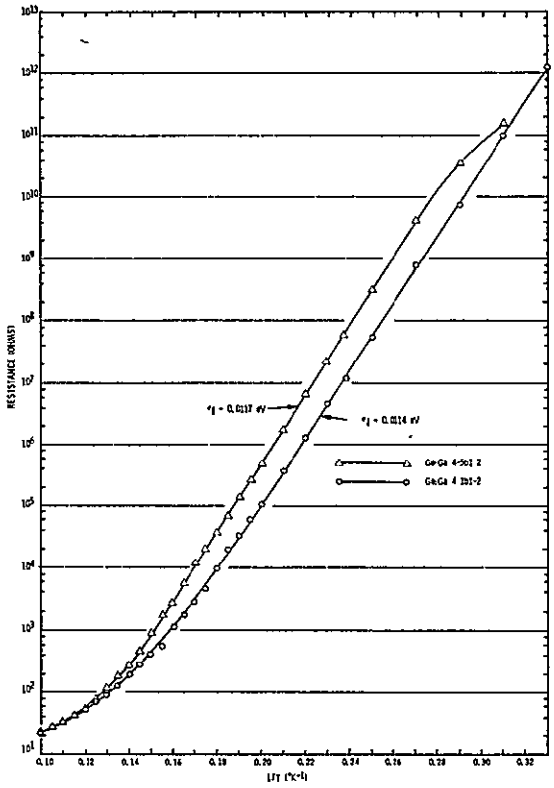

Figure 3-7. Resistance Versus Reciprocal Temperature for Two Ge:Ga Detector Samples from Crystal 4 ($Q_B \approx 0$)

Also to be noted in Figure 3-7 is the difference in resistance between these two samples. In the temperature range between 3.5° and 5°K, this difference amounts to a factor between 5 and 6. Since both detector samples were cut to the same dimensions and the hole mobility is the same in each, this implies a difference in the free-hole concentration of a factor between 5 and 6. In the temperature range of interest, the free-hole concentration is given by

$$p = \left(\frac{N_A - N_D}{N_D}\right) \frac{2}{\delta} \left(\frac{2\pi m^* kT}{h^2}\right)^{3/2} \exp(-\epsilon_i/kT). \qquad (4)$$

where N_A is the acceptor (Ga) concentration, N_D is the residual donor concentration, k is Boltzmann's constant, h is Planck's constant, ϵ_i is the Ga ionization energy, and δ is the ground state degeneracy of the Ga atom.

Differences in free-hole concentration will be controlled by the acceptor and donor doping concentration factor $(N_A - N_D)/N_D$. From Table 3-1, using values for N_A and N_D from slices 4-1a and 4-5a (which were cut adjacent to samples 4-1b and 4-5b) we calculate from this equation that the free-hole concentration should differ by a factor of 6.2, and the sample with the lowest N_D value (4-1b1-2) will have the highest free-hole concentration and, therefore, the lowest resistance. This is in good agreement with the measured resistance data of Figure 3-7. These resistance data are therefore confirming evidence for the lower residual donor impurity concentration in the seed end of Ge:Ga crystal No. 4.

The ionization energies calculated from the slope of these resistance versus 1/T curves are in good agreement with the values obtained from Hall coefficient data.

Section 4

Ge:Be CRYSTAL GROWTH AND EVALUATION

Ge:Be CRYSTAL GROWTH

The initial Ge:Be crystals produced on this program were grown in the same zone melting furnace used for Ge:Ga crystal growth. This furnace was equipped with two doping spoons so that the doping alloy can be added to the melt without opening the furnace to laboratory air. Crystals were grown in an atmosphere of hydrogen gas purified by passage through a hot palladium membrane. A Ge:Be doping alloy of approximately 0.01 atom percent was prepared by melting together the appropriate amounts of high purity Ge and Be in a quartz tube under hydrogen gas.

In the first crystal growth run, an amount of doping alloy was used sufficient to produce about 10^{15} Be atoms/cm^3 in the grown crystal. The calculation was based on a value for the distribution coefficient of Be in Ge of 0.07 as reported by Shenker, et al.[5] It turned out that no Be was detected by Hall effect measurements on the grown crystal. Four more doping runs were made with ever increasing additions of the Be doping alloy with essentially the same result – no electrically active Be in the grown crystal. Finally, on the sixth and seventh attempts, using an exceptionally large amount of doping alloy, we were able to observe Be in the 10^{16} atoms/cm^3 range. However, the concentration decreased rapidly in the direction along the crystal away from where the doping pellets were placed and, after about 1 inch, no more Be was detected.

From these results, it was concluded that Be must be going into the crystal, but most of it was being made electrically inactive by combining with something, probably oxygen. The observation of an abnormal surface

---

5. H. Shenker, E. M. Swiggard and W. J. Moore, Trans. Metallurgical Soc. of AIME, 239, 347 (1967)

film on the top of the Ge:Be ingots was taken as possible evidence of BeO which floats to the surface of the melt. In addition, Be atoms could be complexed with oxygen in the bulk of the crystal. This has been shown to occur with boron-doped germanium.[6]

A check for Be and O in the bulk of the crystal was made using the mass spectrographic analysis method. Three samples were evaluated; one from crystal Ge:Be 5, and two from crystal Ge:Be 6. Crystal Ge:Be 5 showed no electrically active Be in a Hall effect measurement. Crystal Ge:Be 6 showed electrically active Be in one sample (S-1), but essentially no Be in the other.

The results of the mass spectrographic analyses are shown in Table 4-1. Because of interference from the $_{72}Ge^{+8}$ line, the detection of Be is somewhat hampered. However, there is clear evidence of Be in sample Ge:Be 6-S-1. The Hall effect measurement on this sample indicated 1×10^{16} atoms/cm^3 of electrically active Be which corresponds to 0.22 ppma. The mass spectrographic analysis indicates 65 ppma; about 300 times the electrically active amount. There is also clear evidence of an ample supply of oxygen in the crystal to complex with the Be. Crystal Ge:Be 5 showed more than twice the oxygen content of Ge:Be 6. Also of interest are the large concentrations of the shallow acceptor atoms, B and Al. These concentrations are much greater than would normally be detected in a Hall effect measurement, and indicate that oxygen complexing is also taking place with these atoms.

From past work,[7, 8] it is known that oxygen is normally present in Ge to a level of about 50 ppma, although it has been noted[8] that the results will vary depending on the method of crystal growth. The mass spectrographic analyses on our crystals showed much higher oxygen levels than normal.

---

6. W. D. Edwards, J. Appl. Phys. 39, 1784 (1968)
7. C. D. Thurmond, W. G. Guldner, and A. L. Beach, J. Electrochem. Soc. 103, 603 (1956)
8. H. A. Papazian and S. P. Wolsky, J. Appl. Phys. 27, 1561 (1956)

Table 4-1. Impurity Concentrations in Three Germanium Samples (in parts per million atomic, ppma)

Element	Detection Limit*	Ge:Be 5 S-1	Ge:Be 6 S-1	Ge:Be 6 S-2
Li	0.1	3.6	3.5	0.7
B	0.2	ND	ND	25.5
Be**	10.0**	20.0	65.0	10.0
O	0.3	1372.0	456.0	565.0
Na	0.1	42.0	77.0	30.0
Mg	3.0	~3.0	ND	ND
Al	0.7	35.0	91.5	23.0
Si	0.7	0.7	0.7	0.7
K	0.3	0.3	4.3	2.1
Ca	0.5	2.2	6.4	9.3
Cu	1.0	1.0	ND	ND
Ga	0.1	4.9	5.4	3.8
Ag	1.0	2.2	ND	ND

Note: Tantallum and gold are not reported since tantalum slits and gold foil are used. Gallium is residual in the mass spectrometer. Ge lines interfere with nitrogen and chlorine determination. Other elements not detected have a detection limit of 5 ppma.

*Based on 1×10^{-8} coulomb exposure.

**$_{72}Ge^{+8}$ interferes with Be determination. The figures listed above are estimates based on the theoretical abundance ratio of Ge72 to Ge74 isotopes. (Measurements performed by Technology of Materials, Santa Barbara, California.)

Because of the extensive zone refining done on the Ge before doping, one would have expected a lower oxygen content than normal. From this result, a leak was suspected in the hydrogen purification system. Indeed, a leak was found.

Subsequent crystals were grown under vacuum with the objective being to reduce the oxygen content in the melt by an out-gassing process. Three more crystals were grown during the remainder of this program. Crystal Ge:Be 8 was doped to 2×10^{17} Be atom/cm^3 using a single doping

pellet addition at the seed end of the ingot. Crystal Ge:Be 9 was incrementally doped with Be to five different levels ranging from about 1×10^{14} to 7×10^{15} Be atoms/cm^3. Figure 4-1 shows the doping profiles obtained for these two ingots. In both of these ingots the Be concentration indicated by the Hall effect data was within 50% of the desired concentration. Therefore, it was concluded that Be-O complexing was not a significant problem in these two ingots. To save time, the starting Ge material used for these two ingots was not extensively zone refined. Only 3 to 5 zone passes were made on as-received "intrinsic grade" Ge.

The last ingot grown, Ge:Be 10, was subjected to extensive zone refining before doping. Some trouble was encountered with the doping spoons, however, and the vacuum had to be broken to correct the problem. The zone heaters were turned off at this point. After doping, the measured electrically active Be concentration was found to be significantly less than the desired amount. Therefore, it was assumed that some Be-O complexing occurred in this ingot. Nevertheless, a Be doping of about 1×10^{15} atoms/cm^3 was achieved which was sufficient for detector fabrication and test.

Ge:Be CRYSTAL EVALUATION

Preliminary evaluation of Ge:Be crystals was made by Hall effect measurements at room temperature. Since the Be atom is a double acceptor in Ge with ionization energies of 0.024 and 0.064 eV, each Be atom will contribute two free holes at room temperature. Thus the hole concentration calculated from the measured Hall coefficient must be divided by two to obtain the concentration of electrically active Be centers. A magnetic field strength of 15 kgauss was used in the room temperature Hall measurements. Examples of some of the results of these measurements were given in the previous section.

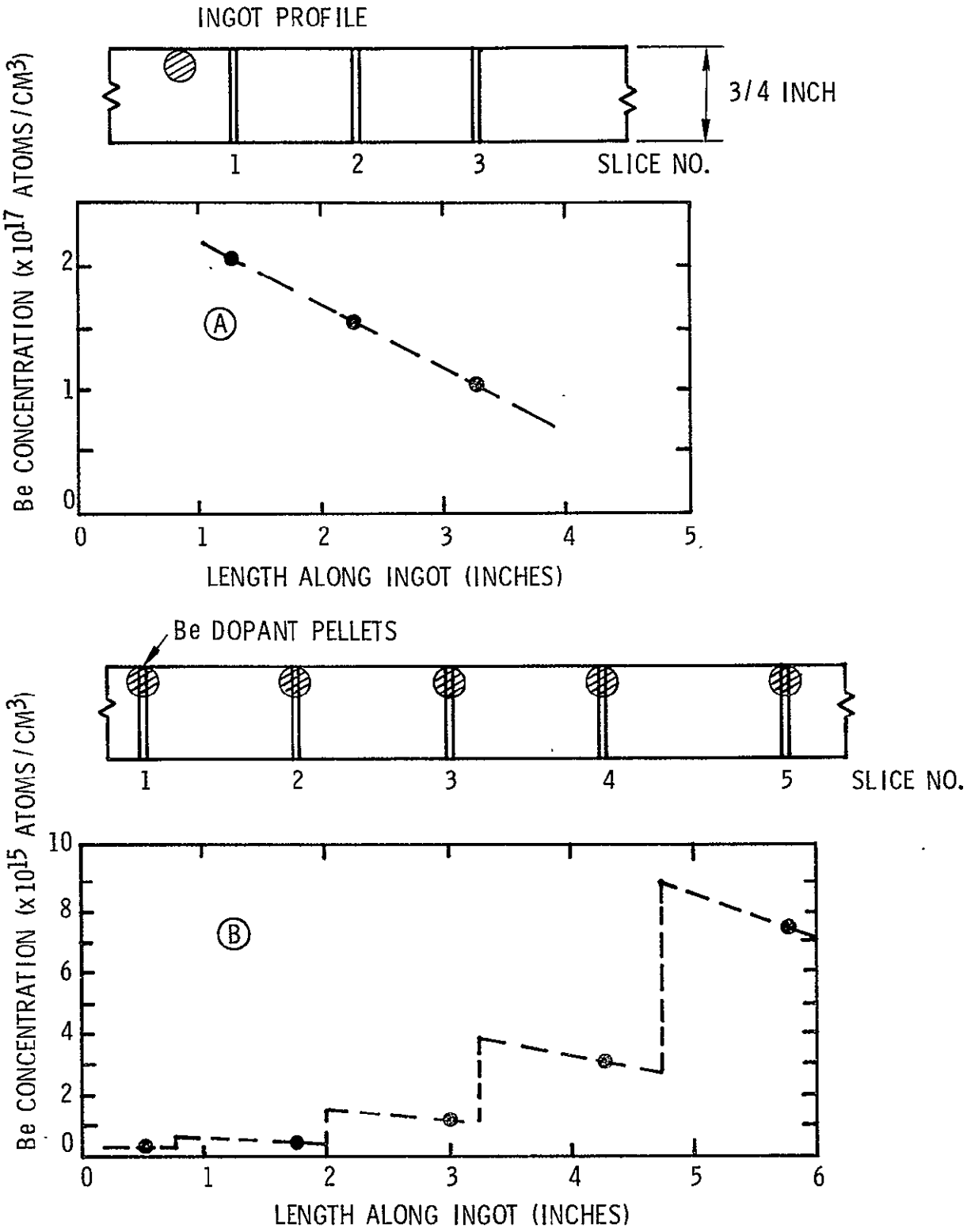

Figure 4-1. Doping Profiles for Two Ge:Be Ingots

Note: A, ingot number 8; B, ingot number 9. Black dots represent measured data points, the dashed line is an approximate interpolation through the measured points.

Selected Ge:Be samples were subjected to Hall effect measurements versus temperature. Analysis of these data provides additional information on the crystal doping parameters such as concentration of shallow acceptor impurities (probably B or Al) and compensating donor impurities. A four-level model was used to analyze the Ge:Be variable temperature Hall data. These levels are: one shallow acceptor, one shallow donor, and the two Be levels. Based on this model, theoretical Hall coefficient curves were generated and fit to the experimental data by adjusting the values of the various dopant concentrations. Further details of this analysis were presented in the previous report.[9]

Figures 4-2, 4-3, and 4-4 show examples of data obtained on Ge:Be crystals 9 and 10. The solid line represents the theoretical fit to the data points which are shown as crosses. Table 4-2 gives the activation energies and doping concentrations used to generate the theoretical curves. In general, the fits to Ge:Be samples were not as good as those made to Ge:Ga samples. This is undoubtedly due to the additional complexity of the four-level model. The value obtained for the Be concentration is quite accurate (± 10%), but values for the shallow acceptor and shallow donor concentrations could possibly be in error by as much as a factor of 2 or 3. Nevertheless, the values obtained are useful for a rough comparison between different crystals.

The shallow acceptor concentration was found to be on the order of 1×10^{13} atoms/cm^3. This is similar to what we have normally found in undoped, zone refined Ge. The shallow donor concentration was quite low, in the 10^{10} to 10^{11} atoms/cm^3 range, similar to what has previously been observed in Ge:Ga crystals.

---

9. See Reference 1.

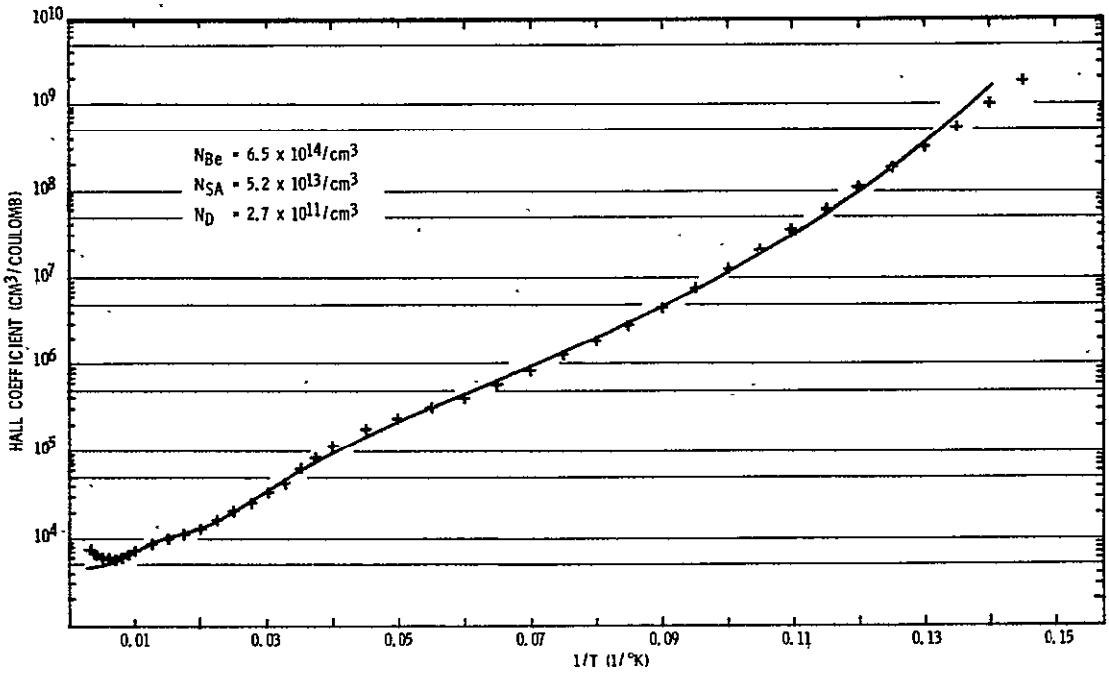

Figure 4-2. Hall Coefficient Versus Reciprocal Temperature for Sample No. Ge:Be 9-2

Note: Crosses are experimental data points, the solid line is theoretical data calculated using the parameters listed in Table 4-2.

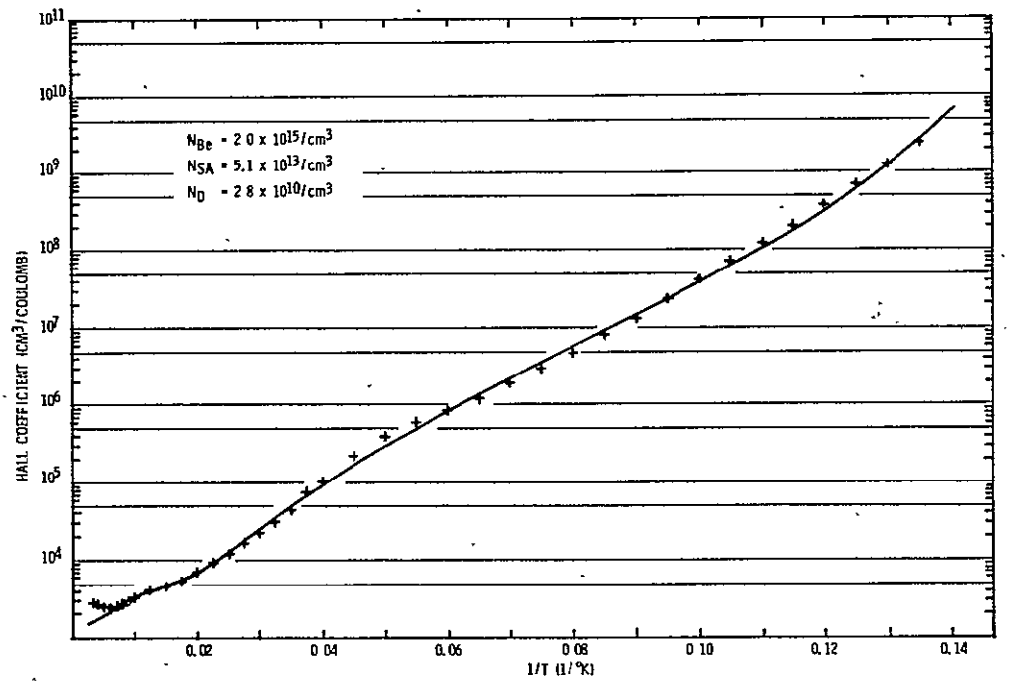

Figure 4-3. Hall Coefficient Versus Reciprocal Temperature for Sample No. Ge:Be 9-3

Note: Crosses are experimental data points, the solid line is theoretical data calculated using the parameters listed in Table 4-2.

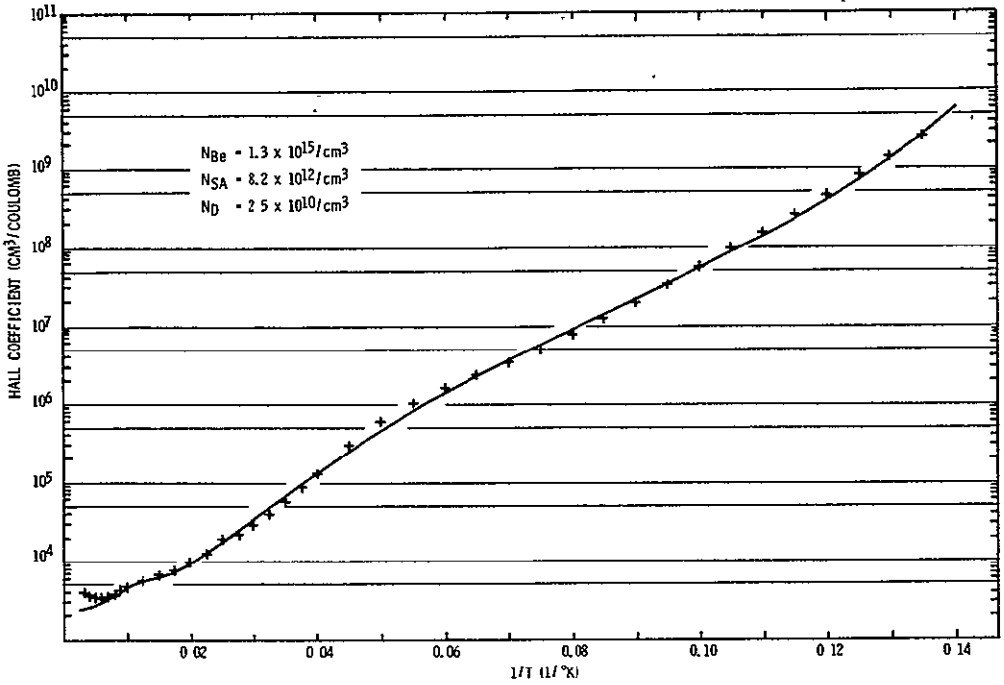

Figure 4-4. Hall Coefficient Versus Reciprocal Temperature for Sample No. Ge:Be 10-3

Note: Crosses are experimental data points, the solid line is theoretical data calculated using the parameters listed in Table 4-2.

Table 4-2. Doping Parameters Obtained from Theoretical Fit of Four-Level Model to Ge:Be Hall Samples

PARAMETER	UNITS	SAMPLE NUMBER		
		9-2	9-3	10-3
$\epsilon(Be_1)$	eV	0.0204	0.0215	0.0214
$\epsilon(Be_2)$	eV	0.0568	0.0699	0.0643
ϵ(SA)	eV	0.0119	0.0142	0.0131
N(Be)	cm^{-3}	6.47 x 10^{14}	1.96 x 10^{15}	1.30 x 10^{15}
N(SA)	cm^{-3}	5.23 x 10^{13}	5.14 x 10^{13}	8.24 x 10^{12}
N(D)	cm^{-3}	2.73 x 10^{11}	2.79 x 10^{10}	2.50 x 10^{10}

ϵ = IONIZATION ENERGY IN eV
N = DOPING CONCENTRATION IN cm^{-3}
Be_1 = FIRST Be ACCEPTOR LEVEL
Be_2 = SECOND Be ACCEPTOR LEVEL
SA = SHALLOW ACCEPTORS
D = SHALLOW DONORS

The ionization energies obtained for the two Be acceptor levels are reasonably close to the previously published values of 0.024 and 0.064 eV. The ionization energy obtained for the shallow acceptor is significantly higher than the accepted literature value of 0.011 eV. A similar result was mentioned previously for the Ge:Ga samples which were tested. The reason for this is not presently known.

HALL MOBILITY

The Hall mobility measured on four Ge:Be samples is shown in Figure 4-5 as a function of temperature. The more lightly doped samples exhibit a continually rising mobility down to the lowest temperature recorded. The sample with the heaviest doping shows a leveling off at a much lower mobility. This is due to neutral impurity scattering.

The low-temperature mobility values of the samples with the lightest doping (Nos. 9-2 and 10-3) are comparable to those measured on the Ge:Ga samples and are still limited by lattice scattering even though the doping concentration in the Ge:Be samples is 3 to 5 times greater. This implies that the neutral Be atom, because of a smaller effective size in the Ge lattice, has a smaller scattering cross section.

RESISTANCE VERSUS TEMPERATURE

A study of resistance versus temperature behavior was made on three Ge:Be samples from crystal 9 and one from crystal 10. The purpose was to check for hopping conductivity at temperatures below 4.2°K. The measurements were made on surplus Ge:Be detector chips using the same circuit arrangement that was used for the Ge:Ga detectors (Figure 3-6). Background radiation was excluded from the samples during these measurements.

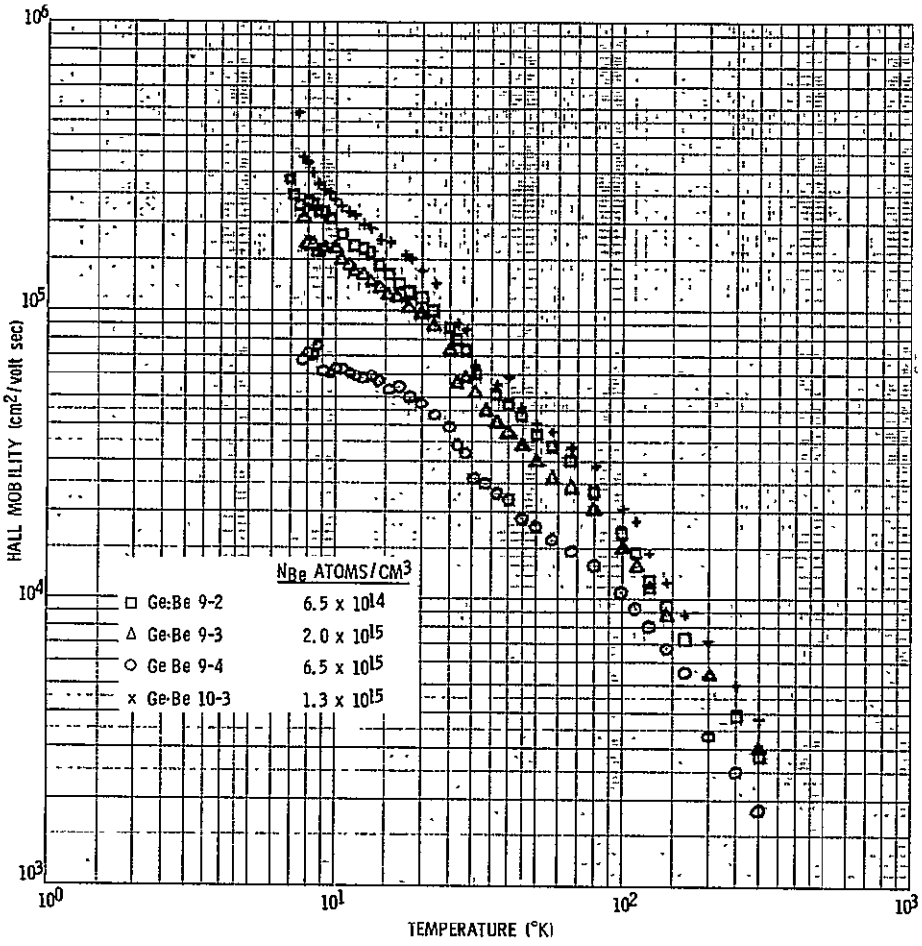

Figure 4-5. Hall Mobility Versus Temperature for Four Ge:Be Samples

The results are shown in Figure 4-6. The sample from crystal Ge:Be 9 with the least Be concentration shows no evidence of impurity hopping conducitivity. As the Be concentration exceeds 1×10^{15} atoms/cm^3, we see a change in slope of the resistance curve at low temperature. For the highest doping concentration of 6.5×10^{15} atoms/cm^3, a pronounced change in slope is observed. This is clear evidence of impurity hopping conductivity. The effect is to lower the sample resistance by roughly a factor of 50 in the low-temperature range. From these data, it appears that the Be concentration in the crystals should be kept below about 2×10^{15} atoms/cm^3 to avoid any serious lowering of detector resistance due to hopping conductivity.

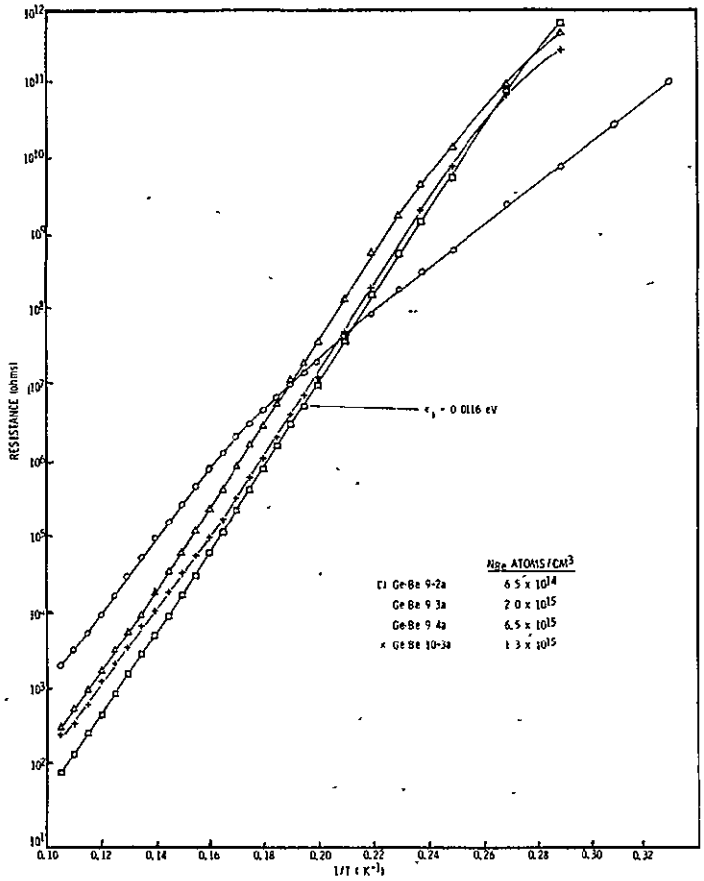

Figure 4-6. Resistance Versus Reciprocal Temperature for Four Uncompensated Ge:Be Detector Samples ($Q_B \approx 0$)

The activation energy determined from the slope of the resistance versus 1/T curves is 0.0116 eV, corresponding to that of a shallow acceptor impurity. This is to be expected because these Ge:Be crystals are not intentionally compensated with donor impurities. Hall effect data presented in the previous section indicated a shallow acceptor concentration on the order of 10^{13} atoms/cm^3. The hopping conductivity is due to electron transfer between Be atoms, however, not between shallow acceptor levels. This, obviously, must be the case because the Be atom concentration exceeds the shallow acceptor concentration by a factor of 650.

IMPACT IONIZATION BREAKDOWN

Using the same test apparatus shown in Figure 3-6 measurements of detector resistance (or conductance) were made as a function of bias voltage (or electric field strength) at two different temperatures. The Ge:Be samples used were the same four on which the resistance versus temperature measurements described in the previous subsection were made. Figures 4-7 and 4-8 show the resulting data plotted as conductance versus electric field strength. Figure 4-7 shows data taken at 4.2°K and Figure 4-8 shows data taken at 3.45°K (with the exception of sample Ge:Be 9-4a which was run at 3.0°K).

These curves show a rather complex behavior; however, they can be understood in a qualitative way. Ohmic conduction occurs only at very low electric field strengths, less than 1 volt/cm. (This is not immediately evident with the scale which was chosen for electric field strength, but was observed). As the electric field is increased, the sample conductance increases due to impact ionization of the shallow acceptor levels. At 4.2°K, the three samples, Ge:Be 9-2a, 10-3a and 9-3a, show this in a very pronounced way. The other sample, Ge:Be 9-4a, does not show this effect so much because it is dominated by impurity hopping conduction. At some relatively high value of electric field strength, impact ionization of the Be atoms commences and the conductance rises very sharply as indicated by the upward pointing arrows. Sample Ge:Be 9-2a could not be biased to the point of impact ionization of the Be atoms because of sample heating which occurred due to its higher conductance. At 3.45°K, a similar behavior is noted, although the shapes of the curves are altered from what they are at 4.2°K. Also to be noted is the increase in the critical field strength for impact ionization of the Be atoms when the temperature is lowered from 4.2° to 3.45°K.

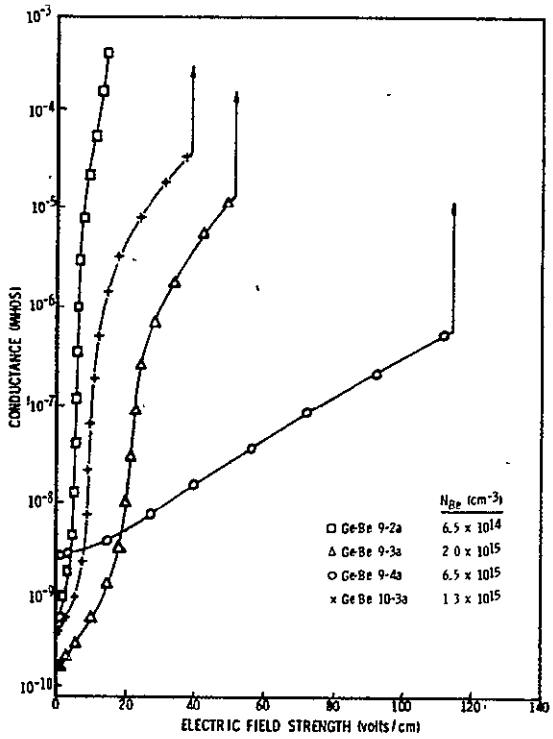

Figure 4-7. Conductance Versus Electric Field Strength for Ge:Be Detector Samples at 4.2°K ($Q_B \approx 0$)

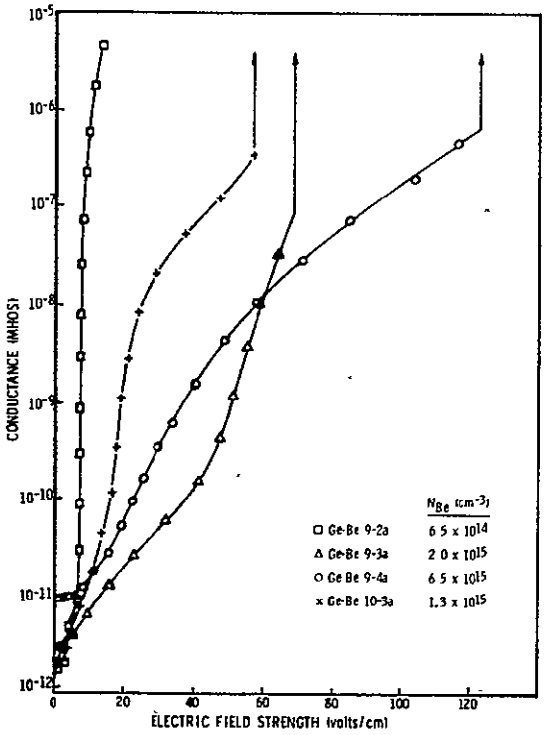

Figure 4-8. Conductance Versus Electric Field Strength for Ge:Be Detector Samples at 3.45°K ($Q_B \approx 0$)

Section 5
DETECTOR FABRICATION AND TEST

DETECTOR FABRICATION

Detector chips were cut from the Ge:Ga or Ge:Be crystals and fabricated into detector elements using standard processing technology which was previously developed at SBRC. Electrical contacts to the detector were formed by ion implantation of boron ions. This produces a p^+-p contact with uniform p^+ doping and a highly planar interface with the p-type crystal bulk. Each detector element was assembled onto a tungsten metal mount along with a load resistor and cryogenic preamplifier. This assembly is shown in Figure 5-1. The load resistor had a nominal value of 5×10^{10} ohms at 3°K. The MOSFET was a Hughes W164 p-channel enhancement mode device.

All Ge:Ga detectors fabricated during this phase of the work were cut from crystal Ge:Ga 4. However, each of the three detectors was made from a different slice so that an evaluation of the whole ingot would be obtained. Detectors were made from slice numbers 1b, 3b and 5b. Figure 3-2 showed the location of these slices in the ingot. The Ga doping concentration in the detectors was 2.5×10^{14} atoms/cm^3. All Ge:Be detectors were fabricated from the same slice of crystal Ge:Be 10. The Be concentration in the detectors was 1.3×10^{15} atoms/cm^3.

LOW BACKGROUND TEST DEWARS

The detector assemblies were mounted to a two-part cooper heat sink which was designed to provide a vise-like clamping of the tungsten detector mount to the copper heat sink. This design was chosen to obtain good thermal conduction to the detector mount. A carbon resistor thermometer was imbedded in a hole drilled into the copper heat sink. Figure 5-2 shows a sketch of the heat sink design.

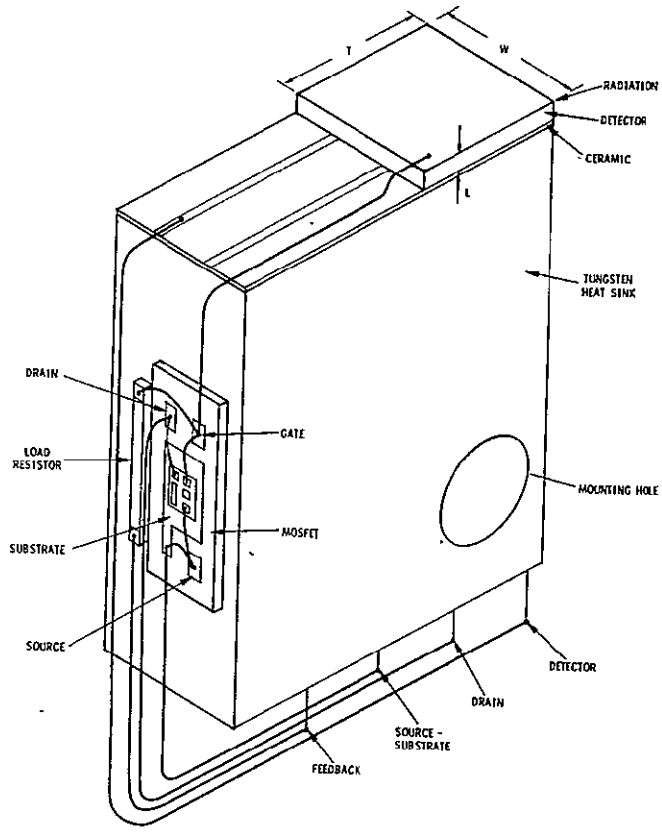

Figure 5-1. Detector — Cryogenic Preamplifier Assembly

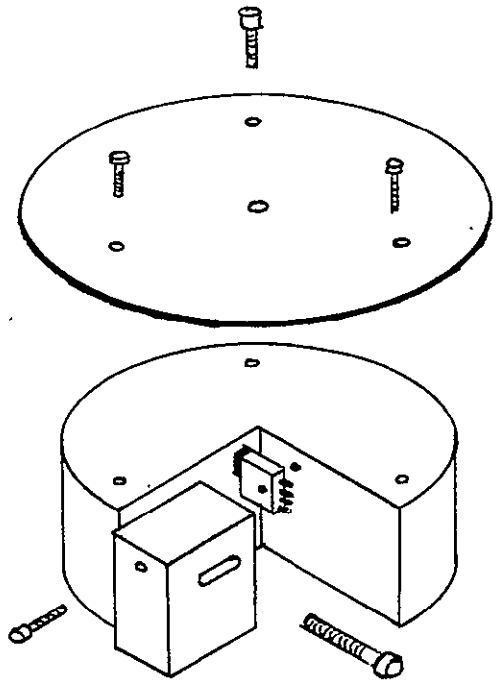

Figure 5-2. Sketch of Copper Heat Sink for Mounting Detector-Preamplifier Assemblies to the Low-Background Test Dewar

This copper heat sink was mounted in a Janis Model RD liquid helium dewar. An aperture defining the sensitive area ($\frac{1}{2}$ mm × $1\frac{1}{2}$ mm) of the detector was placed directly over the detector and a baffle plate with 2.0 mm diameter aperture was placed directly over that. This configuration was used in an effort to prevent stray radiation from getting to the sides of the detector. A series of aperture plates and cold filters were located between the detector and the dewar outer window to provide the desired attenuation of background radiation. Figures 5-3 and 5-4 show the filtering arrangements used in testing Ge:Ga and Ge:Be detectors. Two separate dewars were used to avoid having to take apart the filtering assemblies and thereby possibly cause an irreproducible change in the test set up.

The background photon flux density arriving at the detector plane was calculated from the following formula.

$$Q_B(\Delta\lambda) = Q(300^\circ K, \Delta\lambda)\, T_R \sin^2\theta/2 \qquad (5)$$

where $Q(300^\circ K, \Delta\lambda)$ = photon irradiance from 2π sterradians of 300°K blackbody radiation integrated over the filter pass-band.

T_R = total peak transmittance of all filters.

θ = detector field-of-view angle defined by aperture and distance from detector to aperture.

The details of this calculation for the different low-background conditions used in detector evaluation are presented in Appendix A.

For Ge:Ga, the cold filtering consisted of two special black polyethylene filters and two neutral density filters. The special black polyethylene[10] acts as a long-pass filter with a cut-on wavelength of about 80 μm. It is a scattering filter made by mixing various alkali halide crystal powders together with polyethylene and hot rolling them into a thin film. Some carbon particles also may be in the mixture. The true constituents in the film are not known

10. We are grateful to K. Shivanandan of NRL for supplying us with this filter material and its relative spectral transmittance curve.

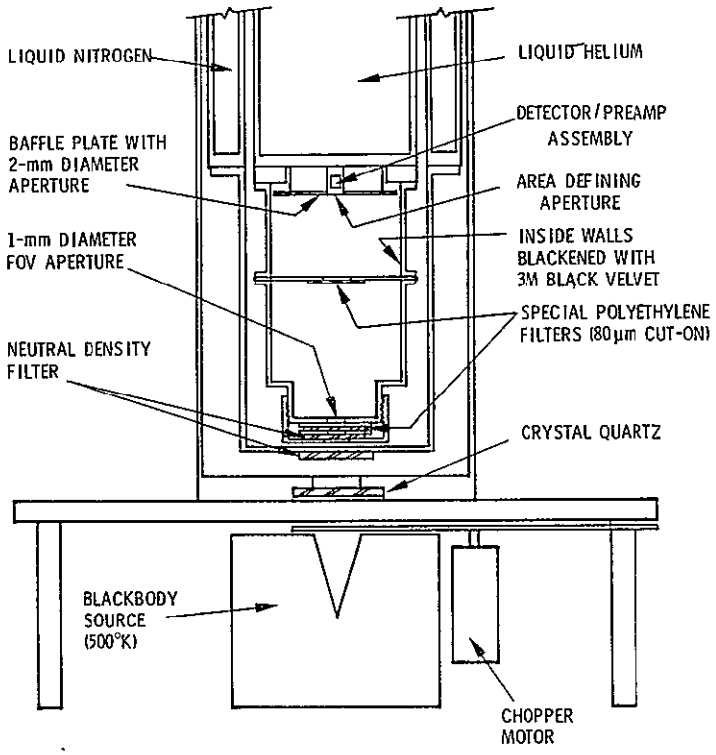

Figure 5-3. Low-Temperature, Low-Background Dewar Setup for Testing of Ge:Ga Detectors at 100 μm

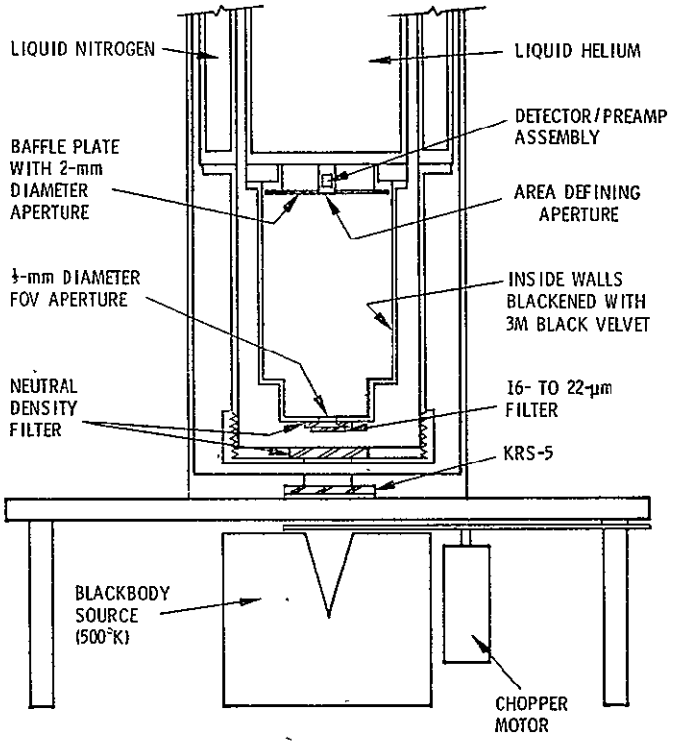

Figure 5-4. Low-Temperature, Low-Background Dewar Setup for Testing of Ge:Be Detectors

to us. The neutral density filters were made at SBRC by evaporating a thin-nichrome metal film onto z-cut crystal quartz flats. The relative spectral transmittance of these filters was not measured, but was assumed to be essentially flat in the 60- to 120-μm range. The average transmittance of these filters was checked at room temperature by placing each filter in front of a dewar containing a Ge:Ga detector (also filtered to detect only radiation beyond about 60 μm) and measuring the attenuation of the detector signal from the 500°K blackbody source.

In most of the Ge:Ga detector testing done on this program, a filter combination was used which gave a calculated background flux $Q_B = 1.2 \times 10^9$ photons/cm^2/sec at the detector plane. Measurements on one detector were made at other background flux levels which were obtained by changing the neutral density filters and field-of-view (FOV) aperture.

For Ge:Be detector testing, a combination of a 16- to 22-μm multilayer interference band-pass filter[11] and two neutral density filters was used. In this case, the neutral density filters were made by evaporating nichrome metal onto germanium flats. This filtering combination had worked well for testing doped Si detectors in past work at SBRC and was easy to implement for the Ge:Be detectors. Admittedly, it would be more desirable to test these detectors in the 30- to 50-μm range; however, a suitable combination of filters for this range was not readily available, so the 16- to 22-μm range was used instead. Extrapolation of NEP data from the 16- to 22-μm range to 50 μm can be made with little additional expected error. The filter combination used for Ge:Be detector testing gave a calculated background photon flux at the detector of $Q_B = 9 \times 10^8$ photons/cm^2/sec.

---

11. Obtained from Optical Coating Laboratories, Inc.

The signal radiation was obtained from a 500°K blackbody located in close proximity to the dewar outer window. A variable speed chopped provided modulation frequencies from 1 to 1000 Hz. The blackbody has a large opening and the detector "looks into" this opening through the small FOV defining aperture located within the dewar. Therefore, the blackbody radiation is effectively emanating from this aperture rather than from the blackbody cavity itself. The blackbody signal irradiance at the detector plane is given by the formula

$$H_{BB}(\Delta\lambda) = \frac{W_{BB}(\Delta\lambda)\, A_{BB}\, T_R F}{\pi D^2} \qquad (6)$$

where $W_{BB}(\Delta\lambda)$ = blackbody radiant emittance integrated over filter passband

A_{BB} = FOV defining aperture area

T_R = total filter transmittance

F = chopper form factor

D = aperture to detector distance

The signal irradiance on the detector is due to the temperature difference between the 500°K blackbody cavity and the room temperature chopper blade (assumed to be at 300°K). Therefore the signal photon flux density impinging on the detector is greater than the 300°K background photon flux density. For noise measurements, the blackbody opening is covered with a shutter so that the detector then only sees 300°K background photons.

The blackbody radiant emittance was numerically integrated over the filter pass-band to obtain that fraction $W_{BB}(\Delta\lambda)$ which would pass through the filter. The details of this calculation are given in Appendix B.

The chopper form factor is used to convert peak-to-peak signal irradiance values to root-mean-square values. For the chopper used, this factor had a value of 0.40. A listing of all the parameter values used in Equations (5) and (6) are given in Table 5-1.

Table 5-1. List of Parameters Used in Blackbody Irradiance Calculations

Parameter	Units	Ge:Ga	Ge:Be
$W_{BB}(\Delta\lambda)$	w/cm^2	3.29×10^{-4}	1.53×10^{-2}
A_{BB}	cm^2	7.85×10^{-3}	1.96×10^{-3}
T_R		1.81×10^{-4}	1.0×10^{-4}
D	cm	8.59	6.65
F		0.40	0.40
$H_{BB}(\Delta\lambda)$	$w(rms)/cm^2$	8.05×10^{-13}	8.6×10^{-12}
θ	degrees	0.67	0.43
$Q_B(300°, \Delta\lambda)$	photons/sec cm^2	1.49×10^{17}	6.36×10^{17}
$Q_B(\Delta\lambda)$	photons/sec cm^2	1.2×10^9	0.9×10^9

TEST PROCEDURE

All testing was done in a screen room. Tests were performed using a source follower cryogenic preamplifier and the external circuit components shown in Figure 5-5. The preamplifier output was coupled to a Quan Tech Model 206C amplifier which provided a voltage gain of 10^3. Amplifier frequency response was flat between 1 Hz and 100 kHz. The low-frequency gain was -3 db at 0.5 Hz. Signal and noise readings were taken on a Quan Tech Model 304 Wave Analyzer and also visually monitored on an oscilloscope.

Tests were designed with the object of evaluating detector performance as a function of frequency, voltage, and temperature. Data were taken at 0.5°K increments from about 4.5°K down to 2.0°K. Temperatures below 4.2°K were obtained by pumping over the liquid helium reservoir of the Janis Dewar. A calibrated carbon resistance thermometer mounted in a hole drilled into the copper heat sink shown in Figure 5-2 was used to monitor detector temperature.

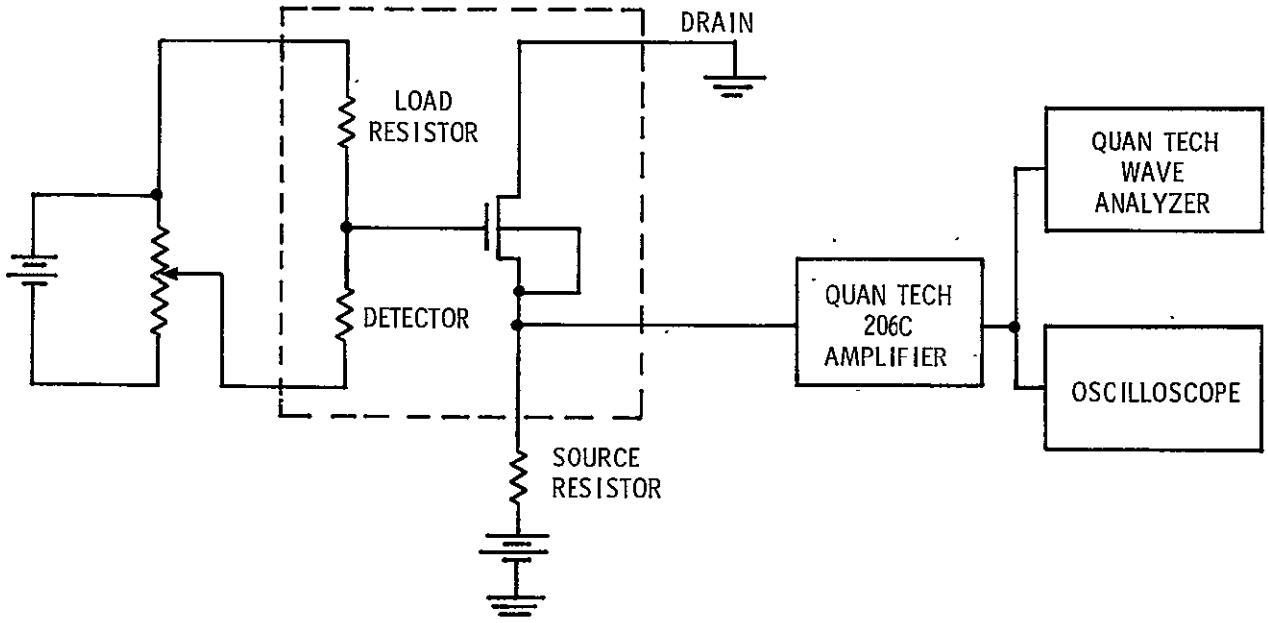

Figure 5-5. Diagram of Circuit Used for Ge:Ga and Ge:Be Detector Tests

Note: Circuit elements within dashed line are at cold temperature, those outside are at room temperature.

Detector bias was first optimized at the highest operating temperature which gave a reasonable signal-to-noise (S/N) ratio. This was usually around 4.0°K. The temperature was then reduced in 0.5° increments. At each new temperature setting, signal, noise and resistance measurements were taken at 10 Hz with optimum bias. At 3.0°K and 2.0°K a more detailed look at detector performance was made. At these temperatures the measurements made were: 1) zero bias noise versus frequency, 2) signal and noise versus bias, at 10 Hz, and 3) signal and noise versus frequency at optimum bias.

RESULTS — Ge:Ga DETECTORS

Three Ge:Ga detectors were fabricated and tested during this program. All were made with material from crystal Ge:Ga 4. Detector 4-1b1-1 showed optimum S/N ratio when operated at a bias voltage of 0.035 volt (0.7 volt/cm) while detectors 4-3b1-1 and 4-5b1-1 had an optimum bias of 0.024 volt

(0.5 volt/cm). Detectors 4-1b1-1 and 4-3b1-1 were tested only at one background flux level, namely 1.2×10^9 photons/sec/cm^2. Detector 4-5b1-1 was tested at various different background flux levels. Figures 5-6 through 5-13 illustrate the relationship between bias voltage, resistance, signal, noise and NEP of these detectors.

The resistance versus temperature data in Figure 5-6 show the same characteristics as were seen earlier in Figure 3-7. That is, detector 4-1b1-1 has a lower resistance at any given temperature than either 4-3b1-1 or 4-5b1-1. This is due to a lower concentration of compensating donor impurities in this part of the crystal.

Detector 4-5b1-1 shows an increase in resistance with decreasing background flux; however, the magnitude of this increase is less than expected. Since Q_B was decreased by a factor of 3.2, detector resistance should have increased by this factor. Instead, it only increased by a factor of 1.6. From this result, it might be inferred that the calculated background flux level of 3.7×10^8 photons/sec/cm^2 was in error. This could possibly have been the case. However, it also should be pointed out that there can be a substantial error in the resistance measurements reported in Figure 5-6. These are made by an indirect method through the source follower MOSFET circuit. Appendix B describes this method. Also, the temperature measurements could be in error due to the fact that the temperature sensing resistor is not located on the detector, but is some distance away in the copper heat sink.

Figure 5-7 shows the detector behavior as a function of bias voltage at two different temperatures, 2.0 and 3.0°K. Note that at 3.0°, the signal voltage tends to saturate at higher bias. This could be caused by either of two things: 1) the drop in detector ac resistance as bias voltage is increased, or 2) photoconductive gain saturation due to carrier sweep-out. Signal saturation was not observed at 2.0°K operation. Similar results were found on two of the three Ge:Ga detectors tested; a tendency toward signal saturation at 3.0°K, but no such tendency at 2.0°K. This indicates a much lower free-hole lifetime at 2.0°K operation.

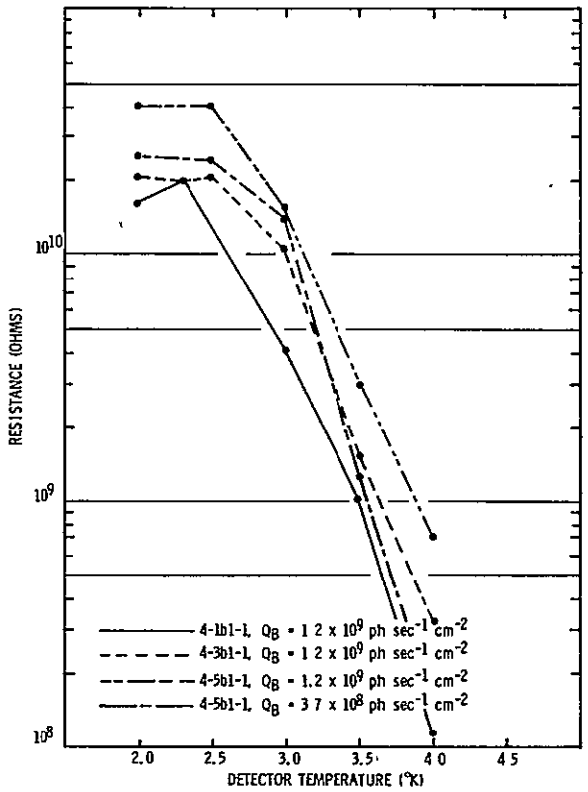

Figure 5-6. Resistance Versus Temperature for Ge:Ga Detectors

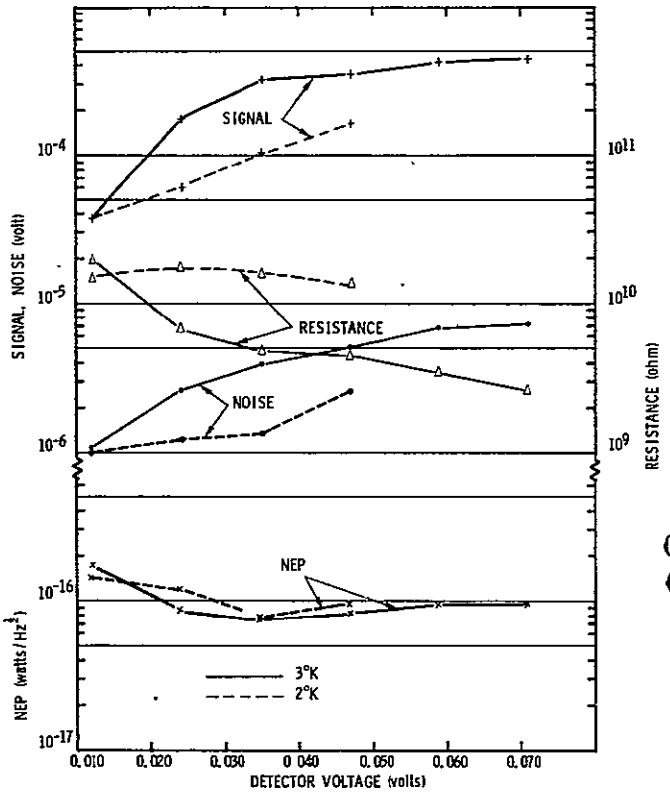

ORIGINAL PAGE IS
OF POOR QUALITY.

Figure 5-7. Signal, Noise, NEP and DC Resistance Versus Bias Voltage for Ge:Ga Detector No. 4-1b1-1 at Two Temperatures (10 Hz Data)

The detector resistance decreases with increased bias. This is due primarily to an increase in free carrier density because of an increasing lifetime with bias.

The noise voltage at low bias is predominantly preamplifier noise. As bias voltage is increased, detector noise becomes evident.

The NEP is higher at low bias voltage because of the preamplifier contribution to the noise. At higher bias, it tends to level off. This is typical of most Ge:Ga detectors that have been tested. Some, however, have shown a clear minimum, and then an increasing NEP at higher bias probably due to an excess detector noise arising at the detector contacts.

The detector signal data in Figures 5-8 and 5-9 can be used to calculate detector responsivity values and from these one can obtain estimates of quantum efficiency and photoconductive gain. The voltage responsivity at wavelength λ is a function of frequency due to the circuit RC rolloff. This frequency dependence can be written as

$$R_v(\lambda, f) = R_v(\lambda, o)\,[1 + (2\pi f \tau_{RC})^2]^{-\frac{1}{2}} \tag{7}$$

where $R_v(\lambda, o)$ is the dc or low-frequency responsivity and τ_{RC} is the circuit response time. By fitting a curve having the functional dependence on frequency shown by this equation to the signal data in Figures 5-8 and 5-9, it was found that the 1-Hz responsivity values are sufficiently close to the dc value to be used in an approximate calculation. The 1-Hz voltage responsivity was calculated from experimentally measured data using the formula

$$R_v(\lambda, 1) = \frac{S(\Delta\lambda)}{H_{BB}(\Delta\lambda) A_D g} \tag{8}$$

where $S(\Delta\lambda)$ = signal voltage measured at output of preamplifier

$H_{BB}(\Delta\lambda)$ = blackbody irradiance at detector (see Table 5-1)

A_D = detector area (7.5×10^{-3} cm^2)

g = preamplifier gain (0.85).

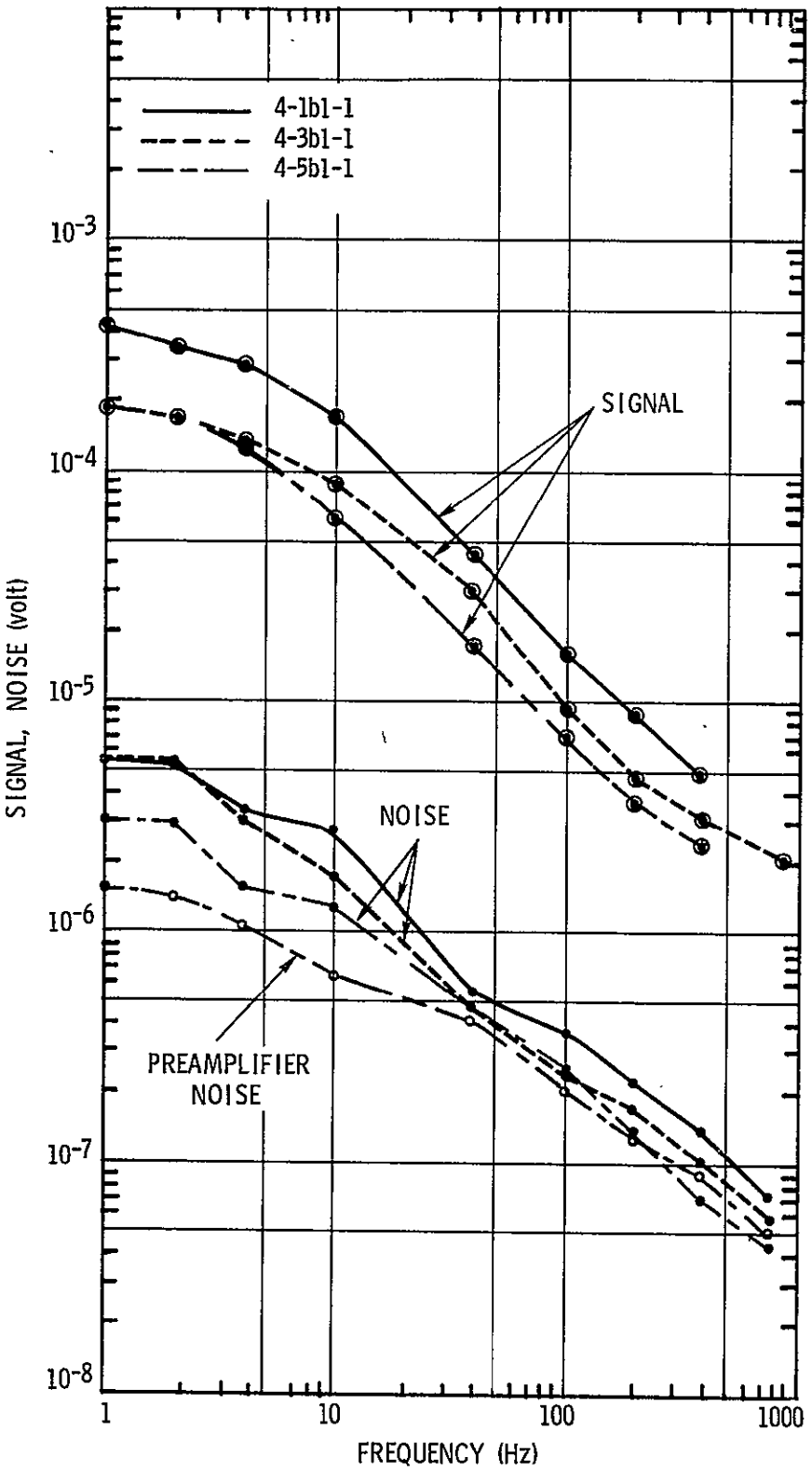

Figure 5-8. Signal and Noise Versus Frequency for Ge:Ga Detectors at 3.0°K

Note: Background photon flux density was 1.2×10^{9} ph sec^{-1} cm^{-2}. Signal and noise values are referred to the output of the MOSFET preamplifier.

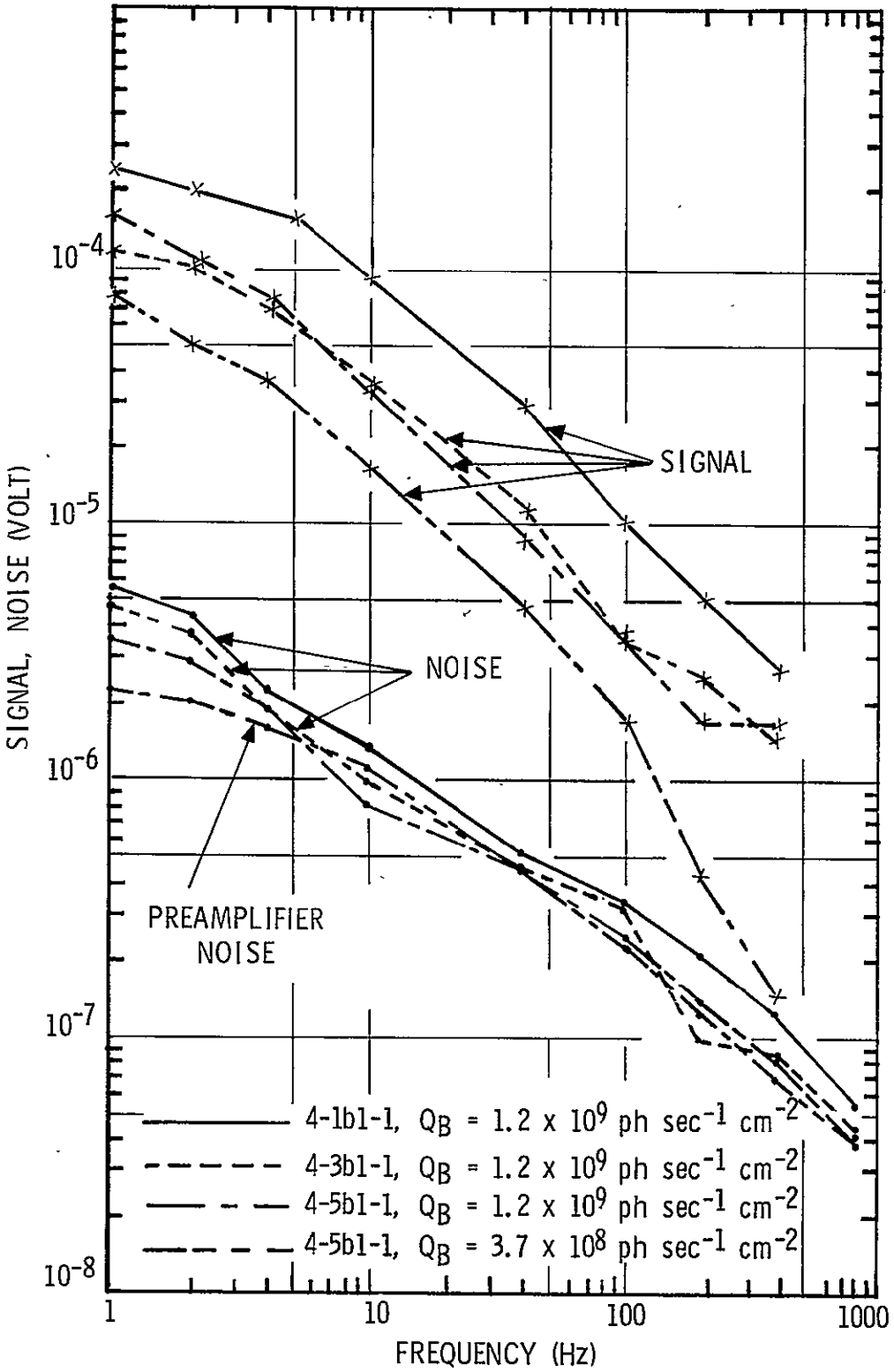

Figure 5-9. Signal and Noise Versus Frequency for Ge:Ga Detectors at 2.0°K

Note: Background photon flux density was 1.2×10^9 ph sec^{-1} cm^{-2}. Signal and noise values are referred to the output of the MOSFET preamplifier.

The short-circuit current responsivity was calculated from the voltage responsivity using the equation

$$I_s(\lambda, 1) = R_v(\lambda, 1)/R_{||} \tag{9}$$

where $R_{||}$ is the parallel resistance formed by the load and the detector ac resistance values,

$$R_{||} = \frac{R_{ac}R_L}{R_{ac} + R_L}, \tag{10}$$

and

$$R_{ac} = R_{dc}\left[1 - \frac{V}{R_{dc}}\frac{dR_{dc}}{dV}\right]^{-1}. \tag{11}$$

According to detector theory, the short-circuit current responsivity is given by

$$I(\lambda, o) = \frac{\eta e \lambda}{hc} G_{pc} \tag{12}$$

where $G_{pc} = \frac{\tau \mu E}{L}$ = photoconductive gain

τ = free-hole lifetime

μ = hole mobility

E = electric field strength

L = interelectrode spacing

η = quantum efficiency

e = electronic charge

λ = wavelength

h = Planck's constant

c = speed of light.

Therefore, once a value for $I(\lambda, o)$ is obtained, some estimates of values for η and G_{pc} can be made.

Using the foregoing equations and the measured experimental data, values of current responsivity were calculated for the three Ge:Ga detectors. The results for operating temperatures of both 2.0°K and 3.0°K are shown in Table 5-2. The current responsivity values are at the peak of the detector's

Table 5-2. Parameters Used in Calculation of Short-Circuit Current Responsivity for Ge:Ga Detectors

PARAMETER	UNITS	DETECTOR NUMBER			TEMPERATURE (°K)
		4-1b1-1	4-3b1-1	4-5b1-1	
BIAS VOLTAGE	VOLTS	0.035	0.024	0.024	2.0 AND 3.0
ELECTRIC FIELD	VOLTS/CM	0.70	0.48	0.48	2.0 AND 3.0
R_{dc}	OHMS	5×10^9	1.0×10^{10}	1.4×10^{10}	3.0
R_{ac}	OHMS	2.8×10^9	7.3×10^9	1.1×10^{10}	3.0
$S(\Delta\lambda, 1)$	MILLIVOLTS	0.44	0.20	0.19	3.0
$R_V(\lambda_p, 1)$	VOLTS/WATT	8.6×10^{10}	3.9×10^{10}	3.7×10^{10}	3.0
$I_S(\lambda_p, 1)$	AMPS/WATT	32 (10)	6.1	4.1	3.0
ηG_{pc}		(0.124)	0.076	0.051	3.0
R_{dc}	OHMS	1.6×10^{10}	2.0×10^{10}	3.1×10^{10}	2.0
R_{ac}	OHMS	1.2×10^{10}	1.3×10^{10}	2.4×10^{10}	2.0
$S(\Delta\lambda, 1)$	MILLIVOLTS	0.23	0.12	0.15	2.0
$R_V(\lambda_p, 1)$	VOLTS/WATT	4.5×10^{10}	2.3×10^{10}	2.9×10^{10}	2.0
$I_S(\lambda_p, 1)$	AMPS/WATT	4.6	2.2	1.8	2.0
ηG_{pc}		0.057	0.027	0.022	2.0

$R_L = 5 \times 10^{10}$ (NOMINAL VALUE)
$\lambda_p = 100\ \mu m$
$A_D = 7.5 \times 10^{-3}\ cm^2$ (1.5 x 0.5 mm)
$f = 1$ Hz

spectral response curve which was taken to be 100 μm. An exceptionally high value of current responsivity was obtained for detector 4-1b1-1 at 3.0°K. No obvious experimental error could be found in the data; however, the result does seem to be spurious. By comparison of the 2.0° and 3.0°K current responsivities of the other two detectors, it appears that a value around 10 amps/watt would be more appropriate for this detector. The current responsivity for this detector would be expected to be somewhat higher than the others because of a higher applied bias and longer free carrier lifetime. Both of these conditions lead to a higher photoconductive gain for this detector. The signal versus bias voltage data shown previously in Figure 5-7 indicate that the photoconductive gain could be on the order of 0.5. (This result is, of course, based on the assumption that the maximum value of the gain at saturation is 0.5.) The use of these results in Equation (12) leads to a

quantum efficiency of 0.25 which seems reasonable considering the Ga doping concentration used in these detectors. The other two detectors probably are operating with a photoconductive gain around 0.2 at 3.0°K. For 2.0°K operation, a decrease in current responsivity by a factor about 2.5 is observed. This must be attributed to a decreased photoconductive gain of the same amount since the quantum efficiency would not be expected to change simply because of a change in operating temperature.

The measured signal-and-noise data was used to calculate the NEP data which is shown in Figures 5-10, 5-11 and 5-12. The NEP versus frequency data shows an essentially flat behavior from 1 to 40 Hz and then rises slowly. An effort was made to measure detector noise data at frequencies below 1 Hz using a spectrum analyzer. The data obtained were unreliable, thus not reported here.

The NEP versus temperature data of Figure 5-12 show a fairly clear minimum at 3.0°K operation. At higher temperatures, NEP increases due to increasing detector generation-recombination noise and decreasing detector resistance. At lower temperatures, the NEP increase is mainly due to a decreased detector responsivity. The conclusion is that the optimum operating temperature is close to 3.0°K. NEP values of about 0.7 to 1×10^{-16} watts/$Hz^{\frac{1}{2}}$ were achieved with a background flux of 1.2×10^{9} photons/sec/cm^2.

One detector, number Ge:Ga 4-5b-1, was also measured at various different background flux levels. Figure 5-13 shows a plot of calculated NEP values versus frequency at four different flux levels. At the highest background flux, NEP rises in the low-frequency range. This is due to 1/f noise in the detector. At the lower background flux levels, NEP shows less dependence on frequency and is reasonably flat down to 1 Hz. The lowest measured NEP was 4×10^{-17} watts/$Hz^{\frac{1}{2}}$ at 1 Hz with a background level of 3.7×10^{8} photons/sec/cm^2.

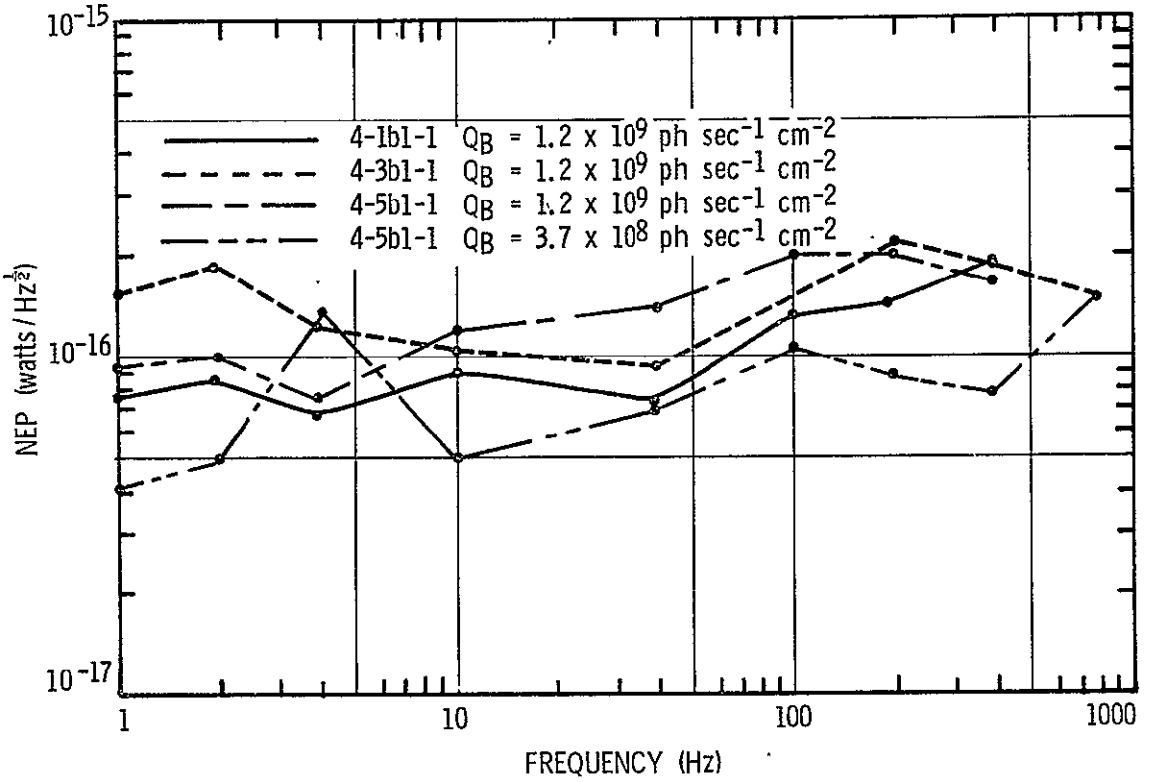

Figure 5-10. NEP Versus Frequency for Ge:Ga Detectors at 3.0°K

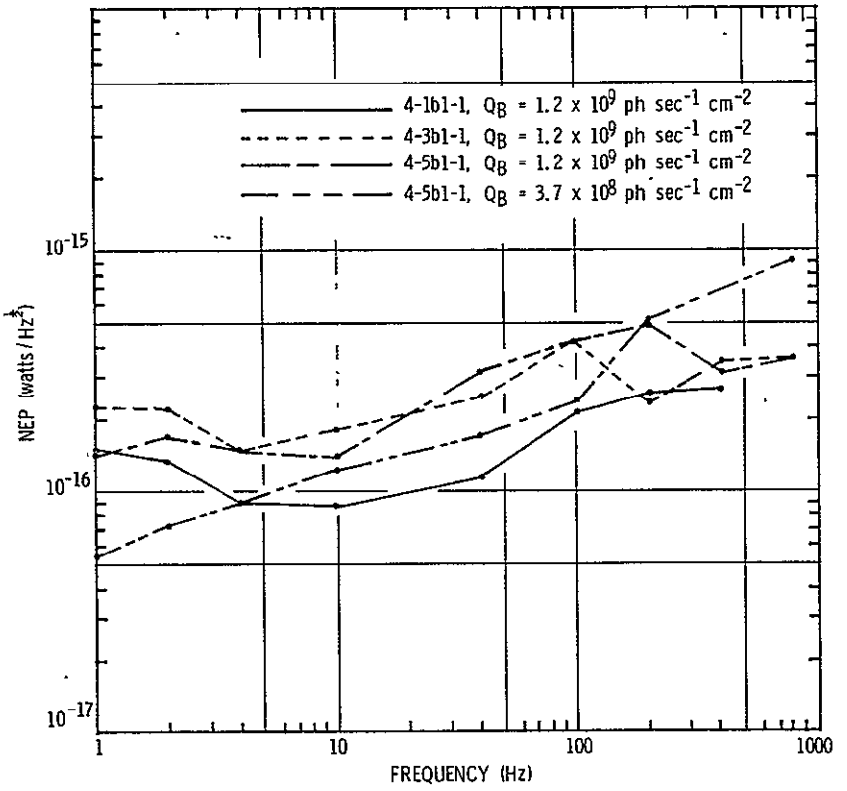

Figure 5-11. NEP Versus Frequency for Ge:Ga Detectors at 2.0°K

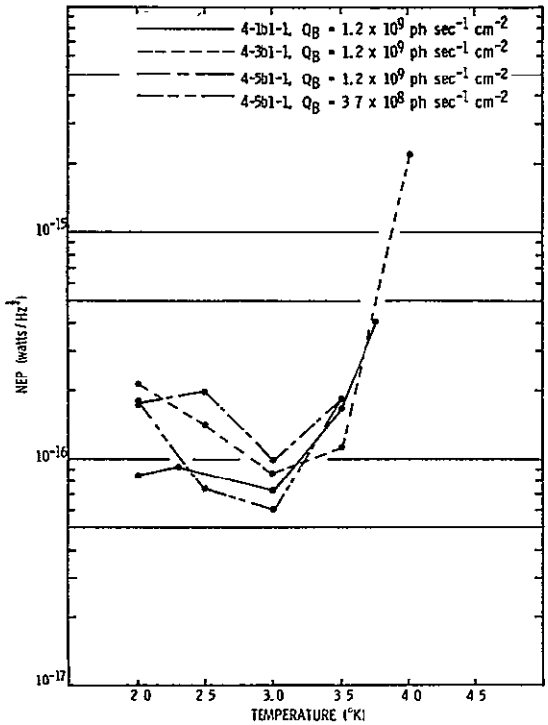

Figure 5-12. NEP Versus Temperature for Ge:Ga Detectors at a Frequency of 10 Hz

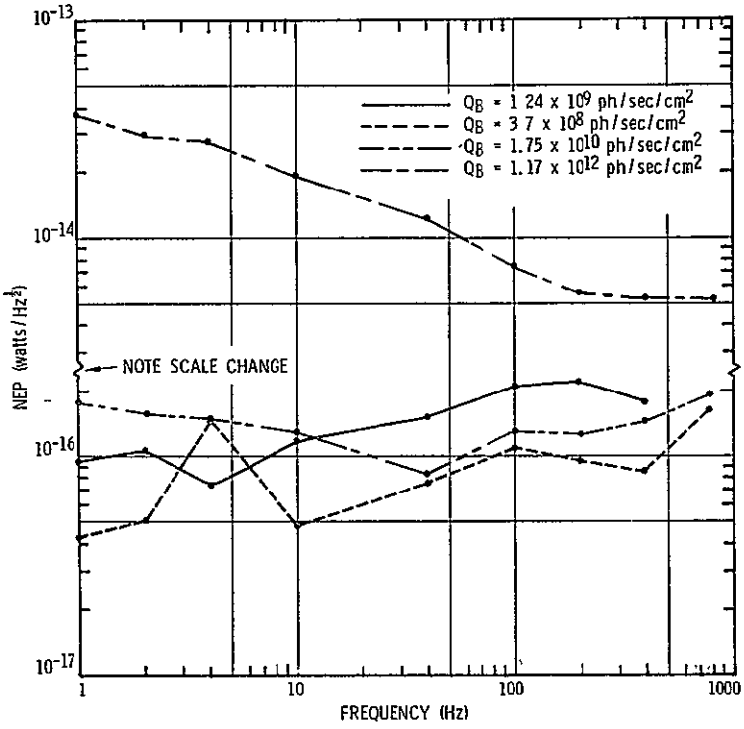

Figure 5-13. NEP Versus Frequency for Ge:Ga Detector 4-5b-1 at 3.0°K for Four Different Background Flux Levels

RESULTS — Ge:Be DETECTORS

As mentioned previously, all three Ge:Be detectors fabricated and tested on this program were cut from the same slice of crystal Ge:Be 10. The slice number was 3a and the location of this slice in the crystal was adjacent to slice 3 from which the Hall sample was taken. The Be doping concentration was 1.3×10^{15} atoms/cm^3. Figures 5-14 through 5-20 illustrate the relationship between bias voltage, resistance, signal, noise, and NEP of these detectors.

In Figure 5-14, the signal is seen to be a linear function of bias voltage and does not tend to saturate as did the Ge:Ga detectors. The resistance is seen to be nearly constant with bias voltage to it can be assumed that R_{ac} is equal to R_{dc}. The NEP is higher at low bias due to preamplifier noise, and then decreases tending to flatten out as bias increases. This is quite evident at 2.0°K operation, but for this particular detector at 3.0°K, the NEP starts rising prematurely due to excess detector noise. The other detectors tested showed the flatter NEP curve at both operating temperatures.

Figure 5-15 shows the measured resistance versus temperature data. The detectors all have similar resistance values as would be expected for detectors cut from the same slice of material. Since this material did not show significant hopping conductivity, the resistance is background photon limited at the lowest temperatures with a value of 2.5×10^{10} ohms. This resistance value is substantially lower than might be expected based on a theoretical calculation. The background limited dc resistance can be expressed as

$$R_{dc} = \frac{L}{\eta Q_B \tau_e \mu w} \qquad (13)$$

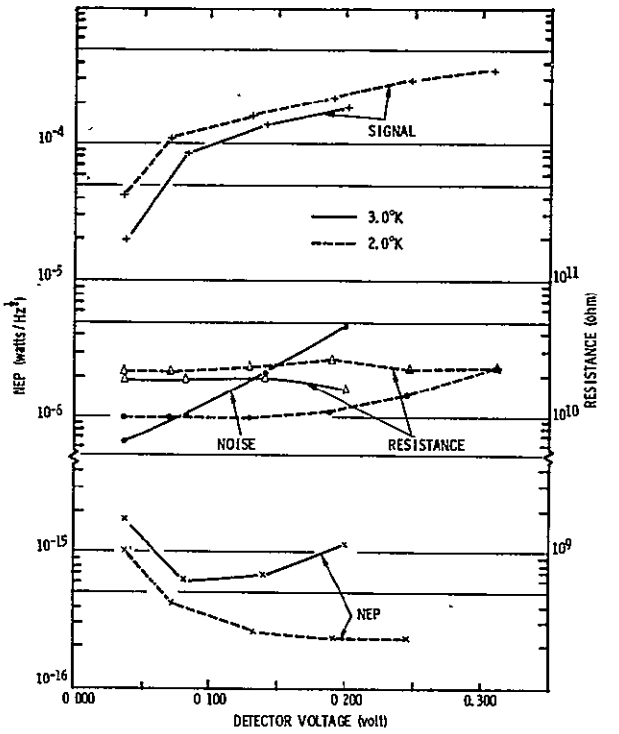

Figure 5-14. Signal, Noise, NEP and DC Resistance Versus Detector Voltage for Ge:Be 10-3a-3 at Two Temperatures, 2°K and 3°K

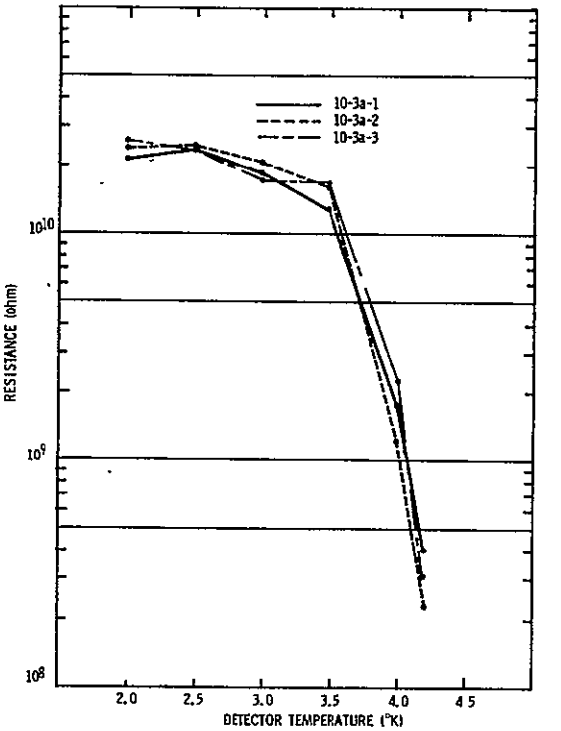

Figure 5-15. Resistance Versus Detector Temperature of Ge:Be Detectors

Note: Background photon flux density was 0.9×10^9 ph sec^{-1} cm^{-2}.

Inserting the following values into this equation:

$L = 5 \times 10^{-2}$ cm

$\eta = 0.3$

$Q_B = 9 \times 10^8$ photons/sec/cm^2

$\tau = 10^{-7}$ sec

$e = 1.6 \times 10^{-19}$ coul.

$\mu = 4 \times 10^5$ cm^2/volt sec

$w = 1.5 \times 10^{-1}$ cm

gives a value for R_{dc} of 1.9×10^{11} ohms, nearly an order of magnitude higher than measured. All the above parameters except η, Q_B and τ came from direct measurements. The η and τ values are reasonable approximations which should be within a factor of 2 or 3 of the true values. It would be necessary to increase the $\eta\tau$ product by a factor of 10 to bring the calculated R_{dc} into agreement with the measured value. This seems to be unreasonable; therefore, it must be concluded that Q_B is actually higher than the stated value of 9×10^8 photons/sec/cm^2.

Figures 5-16 and 5-17 show measured signal-and-noise data versus frequency for two operating temperatures. The signal data can be analyzed in the same way as for the Ge:Ga detectors to obtain short-circuit current responsivity values and estimates of the ηG_{pc} product. The results are given in Table 5-3. The blackbody signal radiation was restricted to the 16- to 22-μm band by a filter. Therefore, direct use of Equation (8) gives the voltage responsivity at a wavelength of about 19 μm. To convert this value to responsivity at the peak of the Ge:Be spectral response which is at 40 μm, the calculated responsivity was multiplied by a factor of 2. This factor is based on the relative spectral response of Ge:Be reported by Shenker, et al.[12] All the values of voltage and current responsivity listed in Table 5-3 are at the detector's peak wavelength of 40 μm. The calculated current responsivity values are seen to be in the neighborhood of 2-5 amp/watt. Detector Ge:Be 10-3a-3

12. See Reference 5.

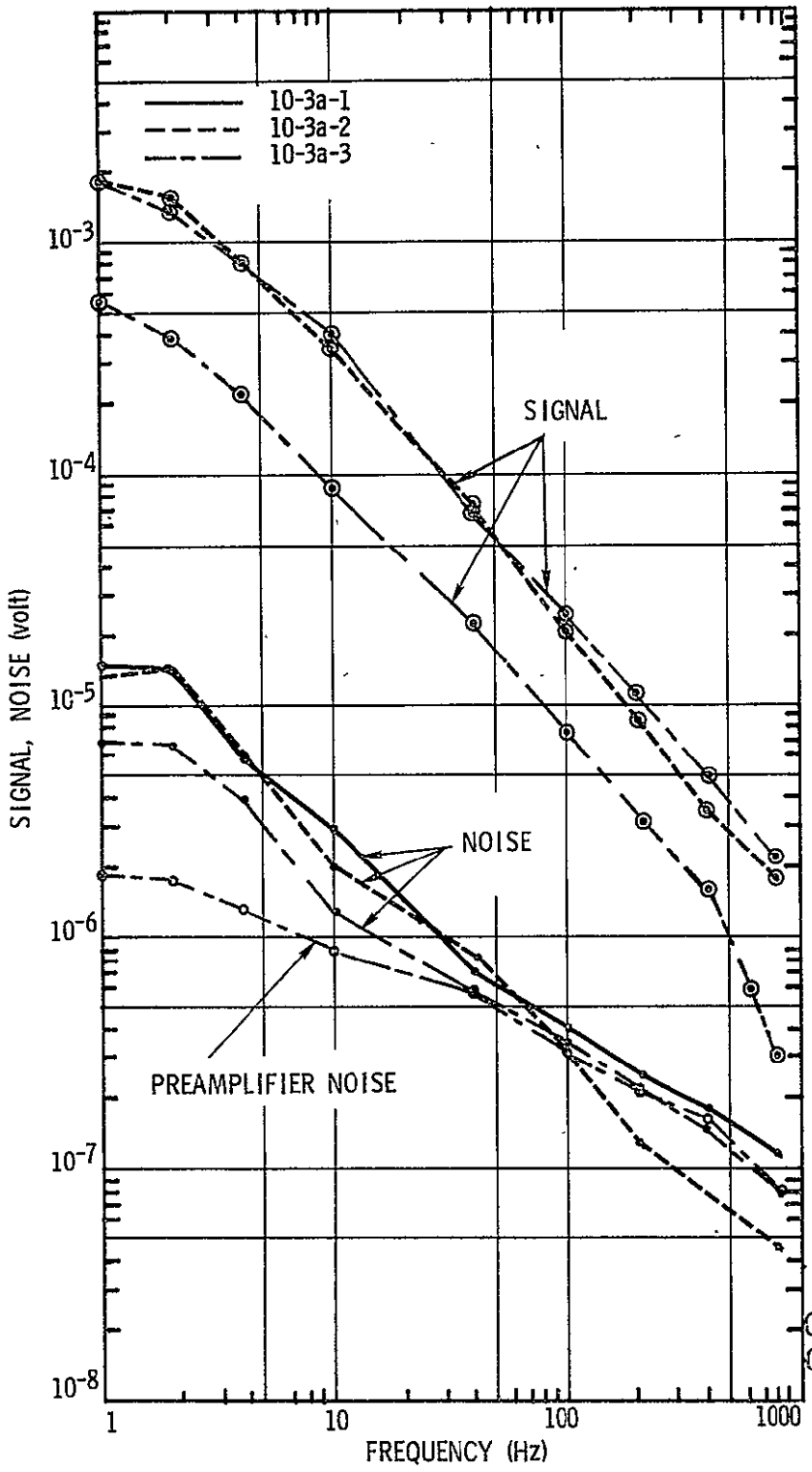

Figure 5-16. Signal and Noise Versus Frequency for Ge:Be Detectors at 3.0°K

Note: Background photon flux density was 0.9×10^{9} ph sec^{-1} cm^{-2}. Signal and noise values are referred to the output of the MOSFET preamplifier.

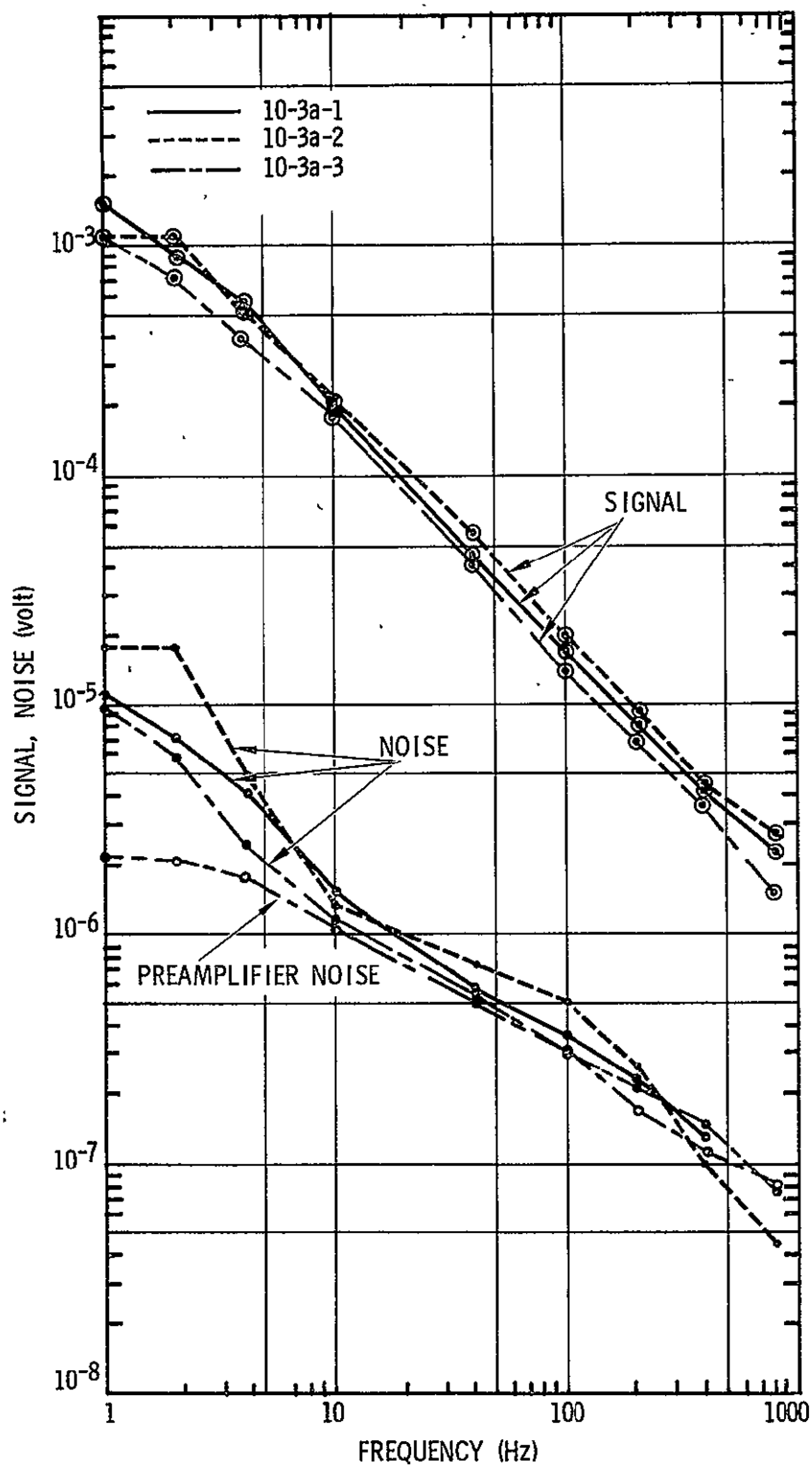

Figure 5-17. Signal and Noise Versus Frequency for Ge:Be Detectors at 2.0°K

Note: Background photon flux density was 0.9×10^9 ph sec^{-1} cm^{-2}. Signal and noise values are referred to the output of the MOSFET preamplifier.

Table 5-3. Parameters Used in Calculation of Short-Circuit Current Responsivity for Ge:Be Detectors

PARAMETER	UNITS	DETECTOR NUMBER			TEMPERATURE (°K)
		10-3a-1	10-3a-2	10-3a-3	
BIAS VOLTAGE	VOLTS	0.235	0.235	0.082	3.0
ELECTRIC FIELD	VOLTS/CM	4.70	4.70	1.64	3.0
R_{ac}	OHMS	1.9×10^{10}	2.2×10^{10}	1.8×10^{10}	3.0
$S(\Delta\lambda, 1)$	MILLIVOLTS	1.8	1.9	0.56	3.0
$R_V(\lambda_p, 1)$	VOLTS/WATT	6.6×10^{10}	6.9×10^{10}	2.0×10^{10}	3.0
$I_S(\lambda_p, 1)$	AMPS/WATT	5.7	5.4	1.8	3.0
ηG_{pc}		0.176	0.167	0.056	3.0
BIAS VOLTAGE	VOLTS	0.259	0.353	0.188	2.0
ELECTRIC FIELD	VOLTS/CM	5.19	7.05	3.76	2.0
R_{ac}	OHMS	2.2×10^{10}	2.6×10^{10}	2.7×10^{10}	2.0
$S(\Delta\lambda, 1)$	MILLIVOLTS	1.5	1.1	1.1	2.0
$R_V(\lambda_p, 1)$	VOLTS/WATT	5.5×10^{10}	4.0×10^{10}	4.0×10^{10}	2.0
$I_S(\lambda_p, 1)$	AMPS/WATT	4.3	2.9	2.8	2.0
ηG_{pc}		0.133	0.090	0.087	2.0

$R_L = 3 \times 10^{10}$ OHMS (NOMINAL VALUE)

$\lambda_p = 40\ \mu m$

$A_D = 7.5 \times 10^{-3}\ cm^2$ (1.5 x 0.5 mm)

f = 1 Hz

was somewhat lower than the other two because it had to be operated at a lower bias voltage. If one assumes a quantum efficiency of 0.3, then the photoconductive gains would be in the range of 0.2 to 0.6. These are reasonably values for the low-frequency gain (1 Hz) which would not be limited by carrier sweep-out.

Calculated NEP values are plotted versus frequency and temperature in Figures 5-18, 5-19 and 5-20. Figures 5-18 and 5-19 show the NEP to be essentially flat with frequency between 1 and 10 Hz, and then rising for higher frequencies. An exception is Detector Ge:Be 10-3a-2 which appears to have some excess noise in the 1- to 2-Hz range causing an increased NEP at these low frequencies.

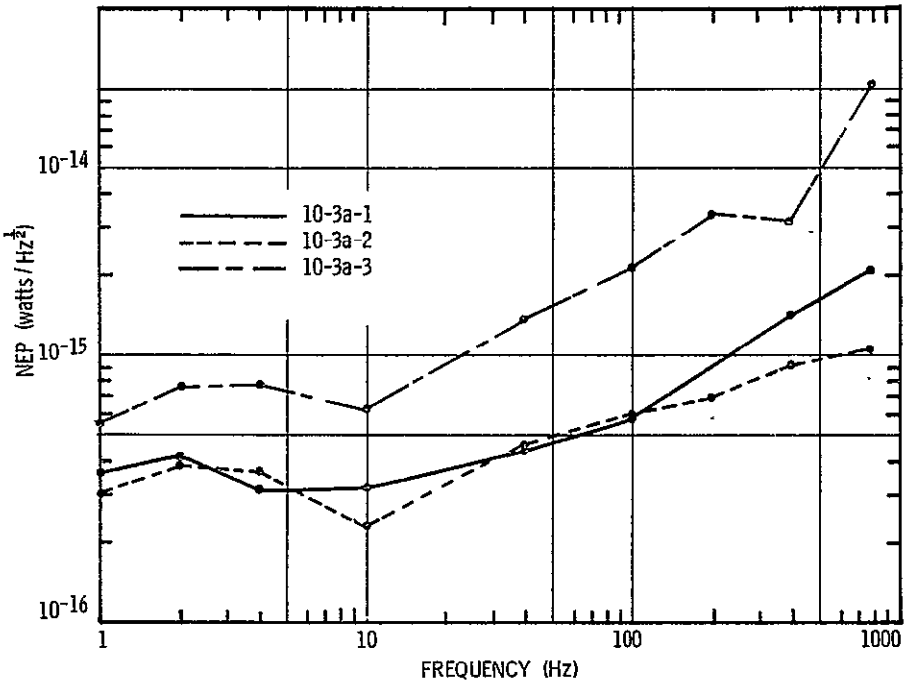

Figure 5-18. NEP Versus Frequency for Ge:Be Detectors at 3.0°K

Note: Background photon flux density was 9×10^8 ph sec^{-1} cm^{-2}.

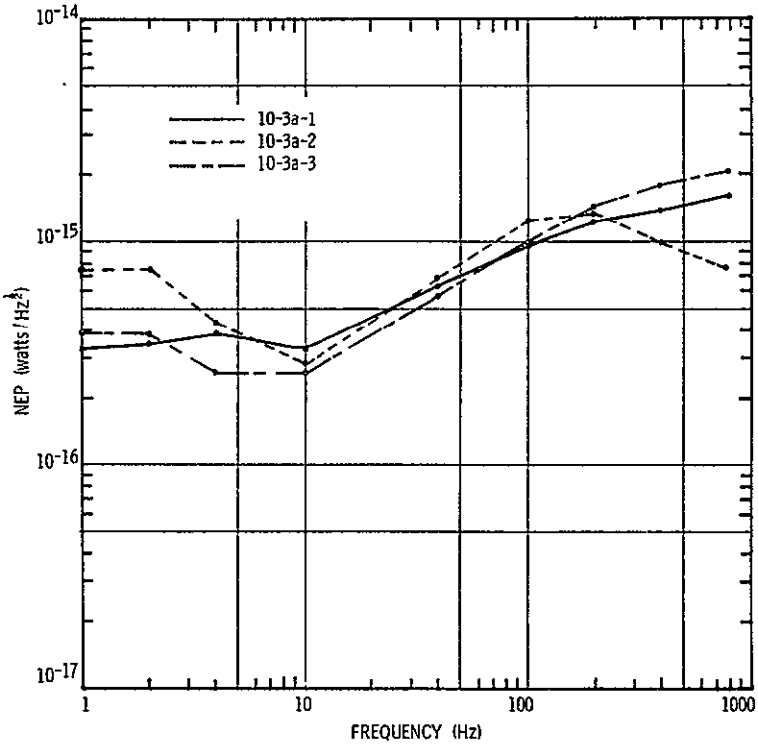

Figure 5-19. NEP Versus Frequency for Ge:Be Detectors at 2.0°K

Note: Background photon flux density was 9×10^8 ph sec^{-1} cm^{-2}.

The NEP versus temperature data in Figure 5-20 show a reasonably flat behavior between 2.0 and 3.0°K and then rise at higher temperature. An exception here is detector Ge:Be 10-3a-3 which reaches its lowest NEP only at 2.0°K. This detector had to be operated at a lower bias voltage than the others because it became excessively noisey at higher bias. This problem was most likely due to contact noise. The minimum NEP is about the same for all three detectors and is 2 to 3×10^{-16} watts/$Hz^{\frac{1}{2}}$.

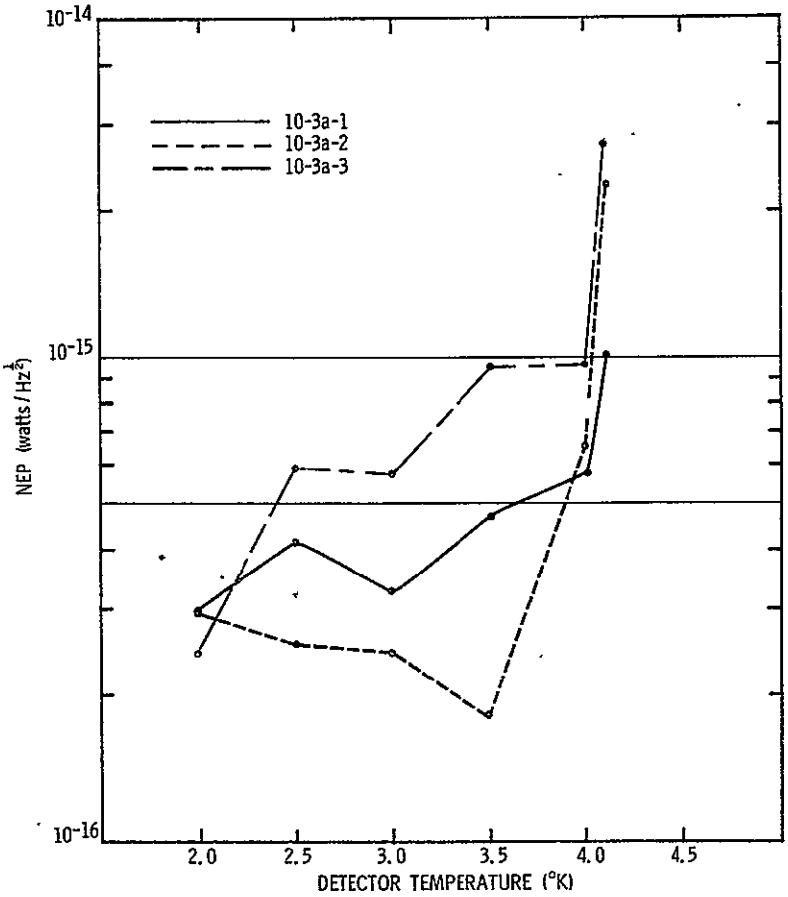

Figure 5-20. NEP Versus Detector Temperature for Ge:Be Detectors

Note: Background photon flux density was 9×10^{8} ph sec^{-1} cm^{-2}.

Section 6

CONCLUSIONS AND RECOMMENDATIONS FOR FUTURE WORK

This work has provided significant advancements in the technology of Ge:Ga and Ge:Be photoconductive detectors for use in astronomical observations at wavelengths from 30- to 120-μm. All the major goals for this phase of the development were accomplished. The primary conclusions that can be drawn from the work performed thus far are as follows.

Ge:Ga DETECTORS

- A Ge purification method was developed which reduces the residual donor impurity concentration to the 10^{10} atoms/cm^3 range. Residual acceptor impurity content may be much higher but is inconsequential to detector performance.
- Introduction of Ga by the zone leveling method was shown to produce a uniformly doped ingot with sufficient material for fabrication of many detectors. The doping concentration can be controlled within an acceptable tolerance.
- Crystals doped to 2.5×10^{14} Ga atoms/cm^3 do not show hopping conductivity. Higher doping concentrations might be useful for increasing the detector's quantum efficiency.
- Short-circuit current responsivity for 100 μm radiation was measured to be in the range of 6 to 10 amps/watt at 3.0°K operation. This implies an ηG_{pc} product of 0.074 - 0.124. Quantum efficiency was estimated to be around 0.25.
- Detectors were not enclosed in an integrating cavity. The use of such a scheme could significantly improve quantum efficiency.
- An NEP of 4×10^{-17} watts/Hz$^{\frac{1}{2}}$ was measured at 1 Hz with a background flux of 3.7×10^8 photons/sec/cm^2 at 3.0°K operating temperature. This compares favorably with the calculated BLIP value of 1.2×10^{-17} watts/Hz$^{\frac{1}{2}}$ ($\eta = 0.30$, $\lambda_p = 100$ μm).
- The NEP is minimized at an operating temperature very close to 3.0°K. Higher or lower operating temperatures may cause a degradation of NEP.
- Reproducibility and yield of good detector elements were excellent for Ge:Ga detectors. Most of the technology development on this material has been completed and the producibility of detectors which meet or exceed the NEP objectives for the IRAS mission has been demonstrated.

Ge:Be DETECTORS

- Oxygen must be eliminated during growth of Ge:Be crystals to prevent Be-O complexing. A vacuum zone melting process was developed which provided a method for doing this.
- The Be concentration should be kept below 2×10^{15} atoms/cm^3 to prevent impurity hopping conductivity from seriously lowering detector resistance at 3.0°K.
- The electric field strength that can be applied to uncompensated Ge:Be is limited to less than 10 v/cm due to impact ionization of shallow acceptor levels.
- Short-circuit current responsivity for 40 μm radiation was measured to be in the range of 2 to 5 amps/watt for 3.0°K operation.
- Detectors were not enclosed in an integrating cavity. The use of such a scheme could significantly improve quantum efficiency.
- The lowest measured NEP for Ge:Be detectors was 2 to 3×10^{-16} watts/Hz$^{\frac{1}{2}}$ at a frequency of 1 Hz with a background flux of 9×10^8 photons/sec/cm^2. The BLIP value for this background is 4.6×10^{-17} watts/Hz$^{\frac{1}{2}}$ ($\eta = 0.3$, $\lambda_p = 40$ μm).
- The NEP is optimized at 3.0°K or lower. There was no clear indication of a minimum in the NEP versus temperature plot.
- The yield of Ge:Be detectors from a given slice of material was acceptable. Two out of three detectors fabricated and tested had reasonably good performance; the third had excessive 1/f noise.
- The uniformity of Ge:Be material properties within a slice is excellent. Uniformity over a whole ingot has not yet been achieved.
- The producibility of Ge:Be detector elements is presently limited by the crystal material uniformity and quality.

RECOMMENDATIONS FOR FUTURE WORK

In the case of Ge:Ga, recommendations for future work could be called minor technological improvements. The work accomplished to date has shown that Ge:Ga detectors can meet the objectives of the IRAS mission. However, minor improvements might still be achieved. For example, Ge:Ga crystals with a Ga concentration greater than 2.5×10^{14} atoms/cm^3 should be grown and evaluated to see if the quantum efficiency can be improved. Also, the use of integrating cavities for improvement of quantum efficiency should be investigated.

Measurements of detector behavior at frequencies below 1 Hz should be made. Although data taken to date show no evidence of any problem in this frequency range, confirming measurements should be made.

In the case of Ge:Be, the crystal growth technology needs further improvement. It is recommended that more work be done in two areas. First, the method of zone leveling to produce a uniform Be concentration along the whole ingot should be implemented. With the existing method, variation of Be concentration along an ingot is still too great to give a sufficient quantity of material for focal plane array production. Secondly, crystals of compensated material should be grown and evaluated to see if they have any advantage over the uncompensated material which has been used in past work. The uncompensated material must be operated at low electric field strengths to prevent impact ionization of the shallow acceptors. In compensated material, electric field strengths 4 to 5 times larger should be permissible. This could give an improvement in photoconductive gain provided that the hole lifetime is not seriously degraded by the additional compensating donors. Careful control will be needed to avoid introduction of too many compensating donors.

As mentioned for the case of Ge:Ga detectors, the use of integrating cavities should also be investigated for Ge:Be detectors. Finally, measurements of detector behavior at frequencies below 1 Hz should also be made.

Appendix A
IRRADIANCE CALCULATIONS

This appendix presents details of the calculation of blackbody signal irradiance and background photon flux density at the detector focal plane in the low-background test dewars.

Ge:Ga TEST DEWAR

As mentioned in Section 5, in the main text, the Ge:Ga detectors were tested using a long-wavelength pass filter consisting of two pieces of "special" black polyethylene and crystal quartz. These materials, along with the detector's natural cutoff at about 120 μm produced a relative spectral response as shown in Figure A-1.* This isolated a spectral band about 35 μm wide in the 100-μm region. Neutral density filters were also used to further attenuate the background photon flux on the detector.

The effective blackbody signal irradiance on the detector was calculated by numerically integrating the blackbody flux over the filter spectral range. To do this, the spectral range was broken up into intervals each 5 μm wide as shown in Figure A-1. The blackbody radiant emittance for each spectral interval was then obtained from a radiation slide rule. These values are shown in Table A-1 along with the spectral intervals and the relative filter transmittance in each spectral interval. Since the signal radiation is produced by the difference between the 500°K blackbody and a 300°K chopper blade, these values were obtained from the slide rule and one was subtracted from the other to obtain the actual signal radiant emittance in each interval. The difference values are listed in column 5 of the table. Multiplication of each number in column 5 by the corresponding relative filter transmittance

*SBRC is indebted to K. Shivanandan of NRL for furnishing these data.

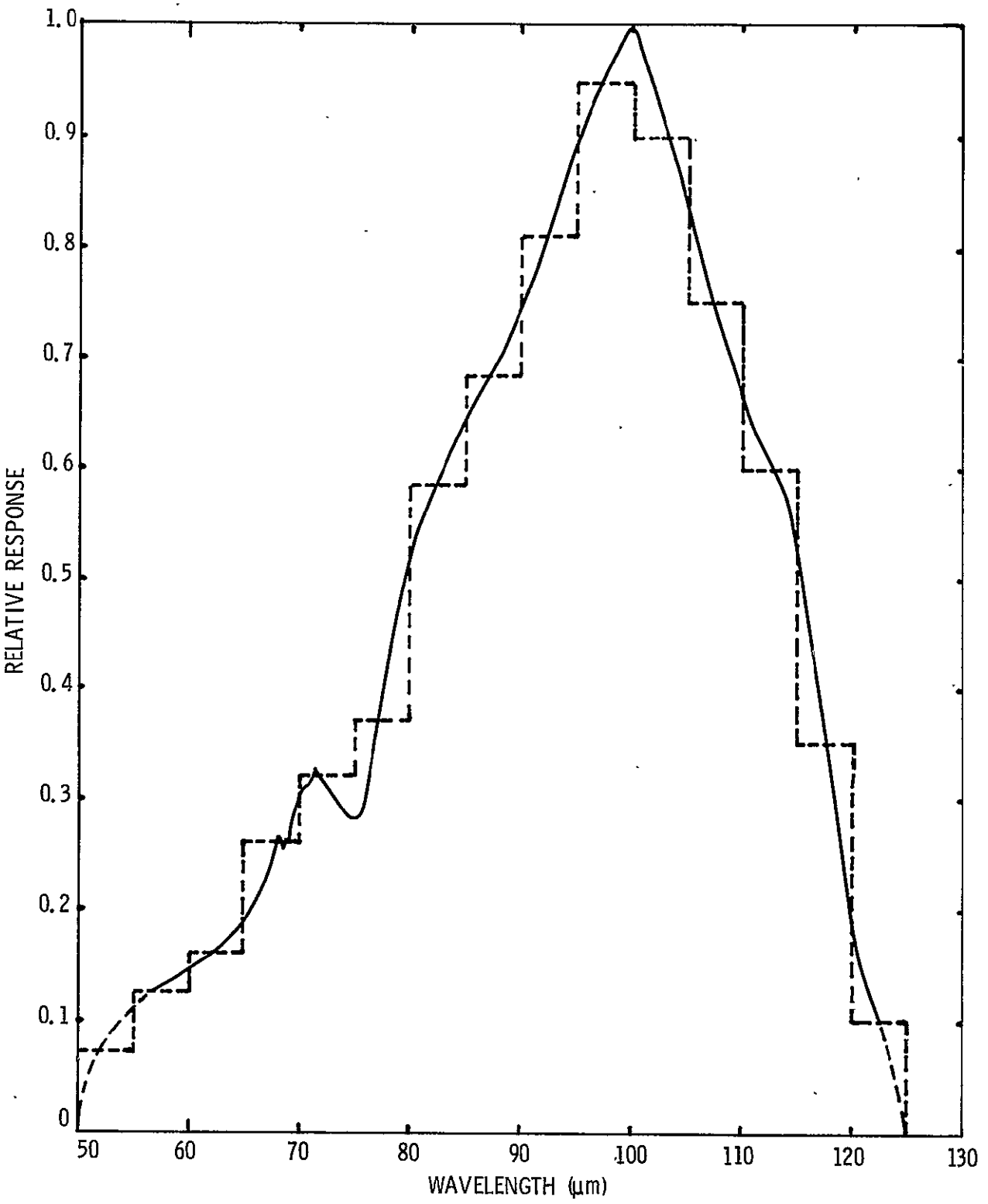

Figure A-1. Relative Spectral Response of Ge:Ga Detector with Long Wavelength Pass Filter

Table A-1. Listing by Spectral Interval of Blackbody Signal Radiant Emittance and Background Photon Flux Values Used for Ge:Ga Detector Testing

(1) λ (μm)	(2) $R_F(\lambda)$	(3) $W_{500}(\lambda)$ (w/cm^2)	(4) $W_{300}(\lambda)$ (w/cm^2)	(5) $W_{500}(\lambda) - W_{300}(\lambda)$ (w/cm^2)	(6) $W_{BB}(\lambda)$ (w/cm^2)	(7) $Q_{300}(\lambda)$ (ph/sec/cm^2)	(8) $Q_B(\lambda)$ (ph/sec/cm^2)
		x 10^{-3}	x 10^{-3}	x 10^{-3}	x 10^{-5}	x 10^{17}	x 10^{16}
40-45	0	1.436	0.670	0.766	0	1.430	0
45-50	0	0.912	0.444	0.468	0	1.060	0
50-55	0.070	0.632	0.310	0.322	2.254	0.818	0.57
55-60	0.125	0.454	0.230	0.224	2.800	0.664	0.83
60-65	0.165	0.334	0.172	0.162	2.673	0.540	0.89
65-70	0.260	0.248	0.130	0.118	3.068	0.441	1.15
70-75	0.320	0.190	0.100	0.090	2.880	0.364	1.17
75-80	0.375	0.150	0.080	0.070	2.625	0.312	1.17
80-85	0.585	0.118	0.062	0.056	3.276	0.257	1.50
85-90	0.685	0.094	0.050	0.044	3.014	0.220	1.51
90-95	0.810	0.076	0.040	0.036	2.916	0.186	1.51
95-100	0.950	0.058	0.032	0.026	2.470	0.157	1.49
100-105	0.900	0.050	0.028	0.022	1.980	0.144	1.30
105-110	0.750	0.040	0.020	0.020	1.500	0.108	0.81
110-115	0.600	0.032	0.018	0.014	0.840	0.102	0.61
115-120	0.350	0.030	0.016	0.014	0.490	0.094	0.33
120-125	0.100	0.027	0.014	0.013	0.130	0.086	0.09
SUMMATION				$W_{BB}(\Delta\lambda) = 3.29 \times 10^{-4}$		$Q_B(300, \Delta\lambda) = 1.49 \times 10^{17}$	

in column 2 gives the effective blackbody radiant emittance in each spectral interval. These values are listed in column 6. Summation overall spectral intervals then gives the total blackbody radiant emittance in the filter pass band.

This total radiant emittance number is then used in Equation (6) to calculate the irradiance at the detector focal plane. Also needed for this calculation are the absolute peak transmittance values for each filter and the dewar window. These are as follows.

	Absolute Peak Transmittance
1 Quartz window	0.85
First neutral density filter	0.015
Second neutral density filter	0.06
2 Special black polyethylene filters	$(0.52)^2$
Atmospheric water vapor	0.88

Total transmittance, $T_R = 1.8 \times 10^{-4}$

A transmittance factor for atmospheric water vapor was also included. Although this produces a small effect on total transmittance, it was found to be not negligible. The effect of atmospheric absorption was checked by flushing the space between the blackbody opening and the dewar window with dry nitrogen. This produced an increase in a Ge:Ga detector's signal by 13%. Since it was impractical to continue flushing this space during all tests, the atmospheric correction factor was applied to the blackbody irradiance calculation.

The equation for signal irradiance, Equation (6) in Section 5, was written as

$$H_{BB}(\Delta\lambda) = \frac{W_{BB}(\Delta\lambda)\, A_{BB}\, T_R\, F}{\pi\, D^2} \qquad \text{(A1)}$$

Substituting the values calculated above, along with those other values listed in Table 5-1, gives

$$H_{BB}(\Delta\lambda) = \frac{(3.29 \times 10^{-4})(7.85 \times 10^{-3})(1.8 \times 10^{-4})(0.4)}{(3.14)\ (8.59)^2} = 8.0 \times 10^{-13}\ \text{w/cm}^2.$$

The background photon flux density at the detector plane was calculated in a similar manner. Column 7 of Table A-1 lists 300°K photon flux density values for each spectral interval as obtained from a radiation slide rule. Column 8 gives the effective values passing through the filter (column 2 × 7) and their sum over all the spectral intervals.

Equation (5) in Section 5 was then used to calculate the background photon flux density at the detector plane. This equation is

$$Q_B(\Delta\lambda) = Q(300°K,\ \Delta\lambda)\ T_R \sin^2 \theta/2. \qquad \text{(A2)}$$

The filter transmittance factor in this case does not include the outer warm quartz window nor does it include the atmospheric water vapor loss. It includes just the two neutral density filters and the two special polyethylene filters. Thus $T_R = 2.4 \times 10^{-4}$. Using this value along with the appropriate values from Tables A-1 and 5-1 gives

$$Q_B(\Delta\lambda) = (1.49 \times 10^{17})(2.4 \times 10^{-4})\left(\frac{0.05}{8.59}\right)^2 = 1.2 \times 10^9\ \text{ph/sec/cm}^2.$$

Ge:Be TEST DEWAR

The Ge:Be Detectors were tested using a 16- to 22-μm multilayer band-pass filter plus neutral density filters on germanium. The relative transmittance curve for this band-pass filter is shown in Figure A-2. The blackbody signal irradiance through this filter was calculated by numerical integration in the same manner as was described for the case of Ge:Ga. Table A-2 lists the relevant data.

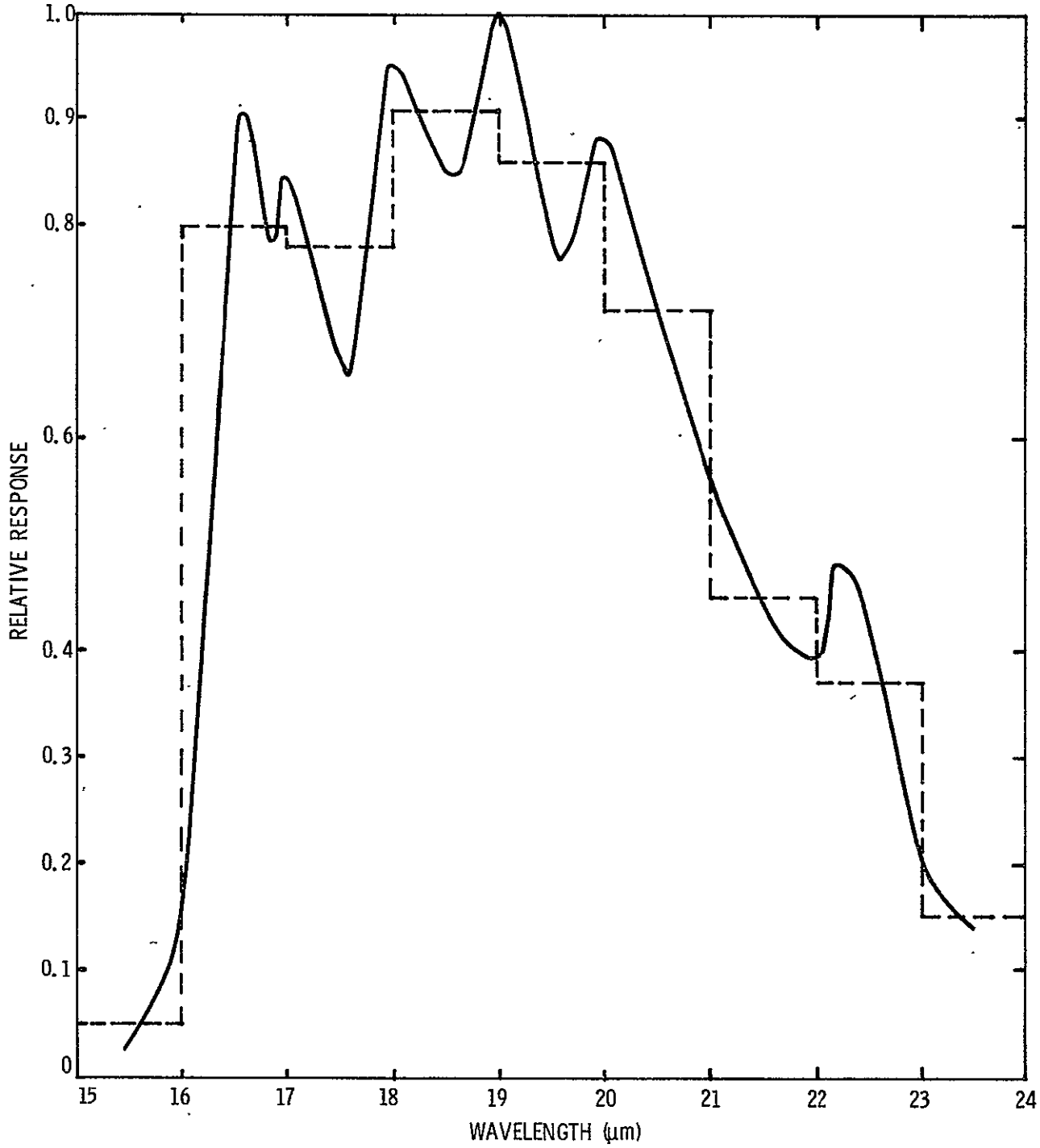

Figure A-2. Relative Spectral Response of Ge:Be Detector with Band-Pass Filter

Table A-2. Listing by Spectral Interval of Blackbody Signal Radiant Emittance and Background Photon Flux Values Used for Ge:Be Detector Testing

(1) λ (μm)	(2) $R_F(\lambda)$	(3) $W_{500}(\lambda)$ (w/cm^2)	(4) $W_{300}(\lambda)$ (w/cm^2)	(5) $W_{500}(\lambda) - W_{300}(\lambda)$ (w/cm^2)	(6) $W_{BB}(\lambda)$ (w/cm^2)	(7) $Q_{300}(\lambda)$ (ph/sec/cm^2)	(8) $Q_B(\lambda)$ (ph/sec/cm^2)
		x 10^{-3}	x 10^{-3}	x 10^{-3}	x 10^{-3}	x 10^{17}	x 10^{17}
15-16	0.05	7.70	2.20	5.50	0.28	1.56	0.08
16-17	0.80	6.30	1.75	4.55	3.64	1.44	1.15
17-18	0.78	5.25	1.52	3.73	2.91	1.40	1.09
18-19	0.91	4.55	1.38	3.17	2.89	1.31	1.19
19-20	0.86	3.85	1.29	2.56	2.20	1.23	1.06
20-21	0.72	3.50	1.10	2.40	1.73	1.15	0.83
21-22	0.45	2.80	0.97	1.83	0.82	1.03	0.46
22-23	0.37	2.45	0.87	1.58	0.58	0.98	0.36
23-24	0.15	2.10	0.74	1.36	0.20	0.90	0.14
SUMMATION				$W_{BB}(\Delta\lambda) = 1.53 \times 10^{-2}$		$Q_B(300, \Delta\lambda) = 6.36 \times 10^{17}$	

Using the data from Tables A-2 and 5-1, and substituting into Equation (A1) gives

$$H_{BB}(\Delta\lambda) = \frac{(1.53 \times 10^{-2})(1.96 \times 10^{-3})(1.0 \times 10^{-4})(0.4)}{(3.14)\ (6.65)^2} = 8.6 \times 10^{-12}\ \text{w/cm}^2.$$

The background photon flux density at the detector was obtained by substituting data from Tables A-1 and 5-1 into Equation (A2) to get

$$Q_B(300°\text{K},\ \Delta\lambda) = (6.36 \times 10^{17})(1.0 \times 10^{-4})\left(\frac{0.025}{6.65}\right)^2 = 9.0 \times 10^{8}\ \text{ph/sec/cm}^2.$$

DETECTOR RESPONSIVITY

The blackbody signal irradiance values calculated in this appendix were used to obtain detector responsivity by the usual formula

$$R_v(\lambda) = \frac{V_S(\Delta\lambda)}{H_{BB}(\Delta\lambda)\ A_D} \tag{A3}$$

where $R_v(\lambda)$ is the responsivity in volts/watt, $V_S(\Delta\lambda)$ is the measured signal voltage, A_D is the detector sensitive area, and $H_{BB}(\Delta\lambda)$ is the effective signal irradiance. It turns out that this procedure yields the responsivity at the peak of the filter spectral distribution λ_p. A derivation of this result is as follows.

If $R_v(\lambda)$ is the detector responsivity at any wavelength and $P\lambda$ is the signal power per unit of wavelength (watts/μm) on the detector at this wavelength, then for a given wavelength range between λ_1 and λ_2, the detector signal voltage will be given by

$$V_S(\Delta\lambda) = \int_{\lambda_1}^{\lambda_2} R_v(\lambda)\ P\lambda\ d\lambda \tag{A4}$$

where $\Delta\lambda$ refers to the spectral interval $\lambda_1 - \lambda_2$.

If the detector's $R_v(\lambda)$ curve is expressed as a relative response normalized to unity as shown in Figures A-1 and A-2, then equation (A4) can be written as

$$V_S(\Delta\lambda) = R_v(\lambda_p) \int_{\lambda_1}^{\lambda_2} RR(\lambda)\, P_\lambda\, d\lambda \qquad (A5)$$

where $RR(\lambda)$ is the relative response (= 1 at λ_p) and $R_v(\lambda_p)$ is the responsivity at λ_p. This equation can be rewritten as

$$R_v(\lambda_p) = \frac{V_S(\Delta\lambda)}{\int_{\lambda_1}^{\lambda_2} RR(\lambda)\, P_\lambda\, d\lambda} \qquad (A6)$$

The integral in the denominator is the same as $H_{BB}(\Delta\lambda)\, A_D$ when $H_{BB}(\Delta\lambda)$ is calculated by the numerical integration method described previously in this Appendix. Therefore, the responsivity calculated from equation (A3) is the responsivity at the peak of the relative spectral response curve λ_p.

Appendix B

DETECTOR RESISTANCE MEASUREMENTS THROUGH MOSFET

This appendix describes the method used for determining detector resistance values when the detector is connected to the cryogenic MOSFET source follower preamplifier.

The circuit diagram is shown in Figure B-1. The detector dc resistance is given by

$$R_{dc} = V_D/I \tag{B1}$$

where

$$I = V_B/(R_L + R_{dc}). \tag{B2}$$

The voltage drop across the detector V_D will appear at the MOSFET source terminal multiplied by the gain of the source follower. This voltage is measured by observing the change in V_S as the detector bias voltage is switched from zero to ON. Thus,

$$V_D = \Delta V_S/0.85 \tag{B3}$$

where ΔV_S is the observed charge in source voltage and 0.85 is the source follower gain. Combining equations (B1), (B2) and (B3) gives

$$R_{dc} = \frac{R_L}{\left(\frac{0.85\ V_B}{\Delta V_S}\right) - 1} \tag{B4}$$

Use of this equation requires prior knowledge of the load resistance R_L. Since the load resistance value can vary with temperature and bias voltage, this may introduce considerable error into the determination of R_{dc} by this method. Values of V_B and ΔV_S can be measured with good precision and will not produce a large error.

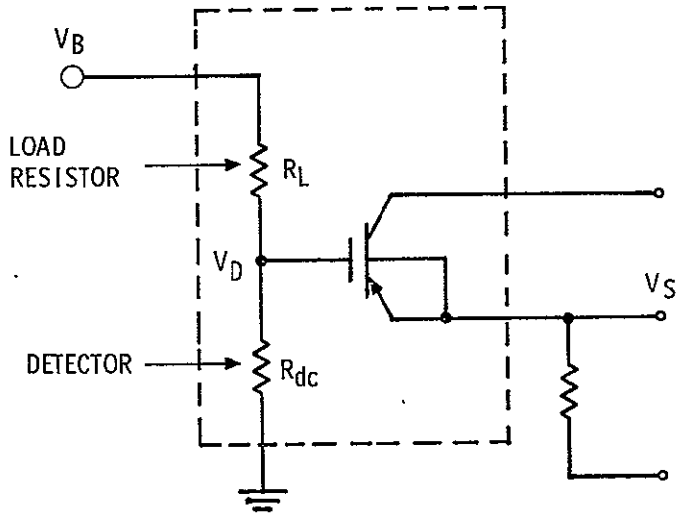

V_B = BIAS VOLTAGE APPLIED EXTERNALLY ACROSS BOTH DETECTOR AND LOAD

V_D = VOLTAGE DROP ACROSS DETECTOR

V_S = SOURCE VOLTAGE

Figure B-1. Circuit Diagram for Low-Background Detector Testing

Table B-1 shows measured resistance values versus temperature and applied voltage for a typical load resistor used in the detector assemblies delivered on this program. It is clear from these data that good calibration of the load resistor must be accomplished to obtain accurate values for R_{dc} from equation (B4).

Table B-1. Resistance Versus Temperature of Typical Load Resistor Used in IRAS Device Assemblies

Temperature (°K)	Resistance (Ω) at 0.020 V	Resistance (Ω) at 0.200 V	Resistance (Ω) at 2.00 V
4.2	3.8×10^{10}	3.7×10^{10}	2.7×10^{10}
4.0	3.7×10^{10}	3.9×10^{10}	2.8×10^{10}
3.5	4.4×10^{10}	4.7×10^{10}	3.2×10^{10}
3.0	5.1×10^{10}	6.0×10^{10}	3.7×10^{10}

Another obvious method for determining R_{dc} would be to attach an additional wire to the detector at the connection to the MOSFET gate and bring this lead out of the dewar. Measurements of detector current and voltage could then be made directly. However, two problems arise with this method. First, the additional lead to the detector produces an added capacitance at the gate input which will cause the circuit response to roll off at lower frequencies. Since the combination of MOSFET gate input and detector capacitance is only about 5 pf, distributed capacitance from the additional wire could easily equal or exceed this value. Secondly, the insulation resistance of the dewar feed-throughs has to be very high; in fact, much higher than the detector resistance. If detector resistance values are in the 10^{10}-ohm range, the insulator resistance should be greater than 10^{12} ohms. The metal-glass feed-throughs used on our dewars can have this high an insulation resistance if properly cleaned and kept dry. However, past experience has shown that they are easily contaminated with use and leakage problems result. It was because of these problems that the indirect method of detector resistance measurement described above was adopted.